This manuscript has not yet undergone peer-review and will be submitted for publication in JOURNAL OF GEOPHYSICAL RESEARCH: ATMOSPHERES. Subsequent versions of this manuscript may have slightly different content. If accepted, the final version of this manuscript will be available via the 'Peer-reviewed Publication DOI' link on the right-hand side of this webpage. Please feel free to contact the corresponding author.

Climate change impacts on surface heat fluxes in a deep monomictic lake

Ana I. Ayala [1,2], Jorrit P. Mesman[1,2], Ian D. Jones[3], Elvira de Eyto[4], Eleanor Jennings[5], Stéphane Goyette[2], and Donald C. Pierson[1]

[1]Department of Ecology and Genetics/Limnology, Evolutionary Biology Centre, Uppsala University, Uppsala, Sweden.

[2]Institute for Environmental Sciences, University of Geneva, 1205 Geneva, Switzerland.

[3]Biological and Environmental Sciences, Faculty of Natural Sciences, University of Stirling, Stirling, UK.

[4]Marine Institute, Furnace, Newport, Co. Mayo, Ireland.

[5]Centre for Freshwater and Environmental Studies, Dundalk Institute of Technology, Dundalk, Co. Louth, Ireland.

ORCID:

Ana I. Ayala: https://orcid.org/0000-0003-3986-5100

Jorrit P. Mesman: https://orcid.org/0000-0002-4319-260X

Ian D. Jones: https://orcid.org/0000-0002-6898-1429

Elvira de Eyto: https://orcid.org/0000-0003-2281-2491

Eleanor Jennings: https://orcid.org/0000-0001-9828-810X

Stéphane Goyette: https://orcid.org/0000-0001-5199-5974

Donald C. Pierson: https://orcid.org/0000-0001-6230-0146

Corresponding author: Ana I. Ayala (isabel.ayala.zamora@ebc.uu.se)

Key Points:

- Future projections of surface heat fluxes in Lough Feeagh under different levels of global warming.
- Significant increases in the annual mean net radiative balance were largely offset by significant increases in the annual mean turbulent fluxes.
- Both spring heating and autumnal cooling significantly decreased under future climate conditions.

Abstract

Turbulent and radiative energy exchanges between lakes and the atmosphere play an important role in determining the process of lake-mixing and stratification, including how lakes respond to climate and to climate change. Here we use a one-dimensional hydrodynamic lake model to assess seasonal impacts of climate change on individual surface heat flux components in Lough Feeagh, Ireland, a deep, monomictic lake. We drive the lake model with an ensemble of outputs from four climate models under three future greenhouse gas scenarios from 1976 to 2099. In these experiments, the results showed

significant increases in the radiative budget that were largely counteracted by significant increases in the turbulent fluxes. The combined change in the individual surface heat fluxes led to a change in the total surface heat flux that was small, but sufficient to lead to significant changes in the volume-weighted average lake. The largest change in total surface heat fluxes were in spring and autumn. Both spring heating and autumnal cooling significantly decreased under future climate conditions, while changes to total surface heat fluxes in winter and summer were an order of magnitude lower. This leads to the counter-intuitive results that in a warming world there will be less heat, not more, entering Lough Feeagh during the springtime, and little change in net heating over the summer or winter compared to natural climate, so that increases in the volume-weighted average lake temperature are largely due to reduced heat loss during autumn.

1. Introduction

Anthropogenic greenhouse gas emissions have increased since the preindustrial period driven by economics and population growth. Associated impacts have been detected throughout the climate system, and in particular for lake systems, influences of the observed global warming have been detected since the mid-20th century (IPCC AR5, 2014). Lakes are considered as sentinels of climate change (Adrian et al., 2009) and the primary observed physical consequences of climate change on lakes are warming surface water temperature (O'Reilly et al., 2015), loss of ice cover (Sharma et al., 2019, 2021), alterations in thermal stability and stratification phenology (Kraemer et al., 2015), changes in evaporation (Gronewold et al., 2014; Okoniewska et al., 2020) and water mass budgets (Smith et al., 2005; Pekel et al., 2016). Ecosystem effects of climate change on lakes have also been observed. Warming water temperature leads to shifts in timing and composition of the phytoplankton community (Rice et al., 2015), including the development of harmful and at times toxic cyanobacterial blooms (Huisman et al. ,2018). Climate change effects also alters fish community size-structure, favoring smaller species and individuals (Jeppesen et al., 2012). Increases in lake thermal stability and duration of thermal stratification result in oxygen depletion in deep water (Jane et al., 2021), which can lead to an increased fish mortality (Till et al., 2019). Anoxic conditions at the sediment-water boundary enhance the nutrient leakage from sediments (North et al., 2014) and can promote an increase in the production (Vachon et al., 2019) and emission of methane (Bastviken et al., 2011), a powerful greenhouse gas. Warming may also have important implications for the ecosystem services that lakes provide, such as drinking water supply, agriculture irrigation, hydroelectricity production, recreation and other amenities (Rinke et al., 2019).

Lake thermal structure has a key influence on most of the processes mentioned above and it is primarily controlled by turbulent (sensible and latent heat fluxes) and radiative (short-wave and long-wave radiation) exchanges of heat between the lake surface and the atmosphere, hereafter referred to as surface heat fluxes, and wind stress (Imboden and Wüest, 1995). Throughflows (advective heat flux; Fenocchi et al., 2017) and sediment exchanges (geothermal heat flux; de la Fuente, 2014) also contribute to the lake heat budget, but their influence is usually minor. Surface heat fluxes are commonly determined based on direct measurements using the eddy covariance technique and a net radiometer (Nordbo et al., 2011) or employing bulk formulae that require lake surface temperature and meteorological data (Woolway et al., 2015; Hipsey et al., 2019).

Solar radiation reaching the lake surface varies according to time of day, season, latitude, weather conditions and local landscape (topography) (Martin and McCutcheon, 1999). Anthropogenic aerosols also play a role affecting incoming solar radiation by affecting atmospheric scattering and absorption. Both declines (global dimming) and inclinations (brightness) in surface solar radiation have been detected worldwide (Wild, 2009). The portion of incoming short-wave radiation, Q_{sin}, reflected by the lake surface is controlled by its albedo. A shortened ice cover period results in a higher absorption of Q_{sin} because open water has a much lower albedo (Li et al., 2022).

The incoming long-wave radiation, Q_{lin}, is the thermal infrared flux from the atmosphere and depends mainly on the atmospheric temperature, moisture, cloud cover and the concentration of the greenhouse gases (GHG) (Livingstone and Imboden, 1989). Long-wave radiation is also emitted from the lake (outgoing long-wave radiation, Q_{lout}) as a function of the fourth power of the absolute lake surface temperature (Imboden and Wüest, 1995). Rising concentrations of CO_2 and other GHG since the preindustrial period have led to an increase in Q_{lin} leading to a warmer air temperature (IPCC AR5, 2014). Heat losses to the atmosphere by long-wave radiation are intensified due to warmer lake surface water temperature.

The latent and sensible heat fluxes, although bidirectional fluxes, are important mechanisms by which the lake transfers absorbed heat back to the atmosphere. The latent heat flux, Q_e, is the energy lost or gained due to evaporation or condensation respectively and depends on the vertical vapor pressure gradient at the air-water boundary. The sensible heat flux, Q_h, is the transfer of heat via turbulent processes between the lake surface and the atmosphere and depends on the vertical temperature gradient at that boundary. Both of these turbulent heat fluxes are also controlled by wind and the static stability of the overlying air. Most of Q_e occurs as evaporation, i.e. lake latent-heat loss, and most of Q_h results in a sensible heat-loss from the lake. Q_e is often the main component of the turbulent heat flux (Schmid et al., 2014). Woolway et al. (2018) analyzed high-frequency data from 45 lakes distributed globally and found that the turbulent heat flux is higher in larger lakes and those situated at low latitudes. The Bowen ratio, B, where $B=Q_h\ Q_e^{-1}$, correlated significantly with latitude, being smaller at low latitude (Q_e increased with decreasing latitudes and Q_h increased with increasing latitudes).

Human-induced climate change is also affecting other essential climate variables, including wind speed and specific humidity. Wind speed showed a significant decreasing trend during 1980-2010 in the northern hemisphere and a significant increasing trend in the southern hemisphere. However, around 2010 the wind trends reversed (Zeng et al., 2019). The decrease in wind speed in the northern hemisphere could be attributed to changes in atmospheric circulation, higher surface roughness (forest growth, land use changes and urbanization) and accelerating Arctic warming, while the increase in wind speed in the southern hemisphere is associated with an intensified Hadley cell (Deng et al., 2021). The specific humidity, the amount of water vapor held in the atmosphere, is increasing rapidly with increasing air temperature given the Clausius–Clapeyron relationship. Observed global mean specific humidity has increased by 0.07 g kg^{-1} $decade^{-1}$ for the period 1973-2002 (Willett et al., 2007). All these changes in the essential climate variables (air temperature, incoming long-wave radiation, solar radiation, wind speed and humidity) have a direct impact on the individual surface heat flux components.

To evaluate the impact of climate change on the lake water environment, numerous climate models have been coupled with one-dimensional hydrodynamical models at global and local scale (Golub et al., 2022). Previous studies have focused on the projected changes in lake water temperature (Shatwell et al, 2019; Ayala et al., 2020), lake heatwaves (Woolway et al., 2021a; Woolway et al., 2022), stratification phenology (Woolway et al, 2021b), loss of ice cover (Woolway et al., 2021c; Grant et al, 2021; Sharma et al, 2021), alterations in mixing regimes (Woolway and Merchant, 2019; Råman Vinnå et al., 2021), evaporation (Wang et al., 2018; Zhou et al., 2021; La Fuente et al., 2022), lake heat content (Weinberger and Vetter, 2014; Vanderkelen et al., 2020), methane production (Jansen et al., 2022) and water management strategies (Mi et al., 2020).

Direct measurements of heat fluxes, in particular turbulent heat fluxes and long-wave radiation loss, at the lake surface are rare and not extensively undertaken, unlike lake water temperatures and meteorological variables, where high frequency monitoring is widespread in many lakes around the world. In addition, turbulent heat fluxes and Q_{lout} depend on surface water temperature, which is successfully reproduced by lake hydrodynamical models (Bruce et al., 2018; Råman Vinnå et al., 2021), and these models are also extensively applied to explore the potential impact of climate change on lake thermodynamics.

Little attention, though, has been focused on the contribution of the individual surface heat flux components to the heat budget and in their seasonal dynamics that strongly affect all of the above-mentioned projected changes. Fink et al. (2014) identified the primary changes in the individual surface heat flux components in Lake Constance for the period 1984-2011 and Schmid et al. (2014) estimated the projected global averaged changes at the end of the 21st century of the individual surface heat flux components. However, how the total heat balance will change under a future climate and how the seasonal dynamics of the individual flux components will evolve, have not been explored and thus deserve attention. Therefore, the purpose of this study was to assess the impact of climate change on (1) the total surface heat flux, (2) the individual surface heat flux components and (3) the seasonal heat flux dynamics in a monomictic, temperate lake for different scenarios of global warming using a one-dimensional hydrodynamic lake model forced by Global Climate Model (GCM) outputs from the Inter-Sectoral Impact Model Intercomparing Project phase 2b (ISIMIP2b). Lough Feeagh is an ice-free, wind-exposed, medium-sized, deep lake located in Ireland close to the Gulf Stream, with a long-term monitoring program. In order to quantify the effect of climate change, the projected surface heat fluxes for the pre-industrial control scenario (natural climate) were compared with the historical scenario and three future scenarios with different levels of warming (Representative Concentration Pathways (RCP): RCP 2.6 (low-emission scenario), 6.0 (medium-high-emission scenario) and 8.5 (high-emission scenario)).

2 Materials and Methods

2.1 Study site

Lough Feeagh (53^{o}56'N, 9^{o}34'W) is a monomictic, oligotrophic and humic freshwater lake located on the west coast of Ireland with a surface area of 3.95 km^{2}, a maximum depth of 46.8 m, an average depth of 14.5 m and an average retention time of 172 days (Hoke et al., 2020).

Ireland's climate is defined as a temperate oceanic climate, on the Köppen climate classification system (Peel et al., 2007). The winters and summers are mild (January mean air temperature 2004–2017: 6.5 °C, July mean air temperature: 14.6 °C) due to the influence of the Gulf Stream. The mean annual precipitation is 1652 mm year^{-1} (2005-2017) with the prevailing wind coming from the Atlantic Ocean to the south-west. Average monthly wind speeds are 5.0 m s^{-1} (Andersen et al., 2020). Lough Feeagh is ice-free all year around and, at present, the lake begins to stratify in April, with peaks in the Schmidt stability occurring towards the end of July, and then fully mixing around the end of October each year (de Eyto et al., 2016).

2.2 Lake model

Simstrat is a one-dimensional model for the simulation of stratification and mixing in lakes. Simulated lake temperature is resolved in the vertical dimension dividing the water column into a fixed number of (not necessarily equally-spaced) layers. The model supports multiple options for external forcing (meteorological variables and total surface heat flux), includes a k-ε turbulence closure scheme and deep seiche mixing (Goudsmit et al., 2002), an ice and snow module (Gaudard et al., 2019), an inflow mixing module (inflow can be added at specific depths or with density-dependent intrusions) and constant geothermal heat flux. Simstrat has been extensively used, with applications covering, for instance, different lake morphometries (Perroud et al., 2009; Stepanenko et al., 2014), future climate scenarios (Råman Vinnå et al., 2021) and extreme weather events (Mesman et al., 2020).

2.3 Climate scenarios

To drive Simstrat and evaluate surface heat flux responses to different levels of warming, we use daily bias-corrected climate model projections from ISIMIP2b (https://www.isimip.org/), specifically projections from GFDL-ESM2M, HadGEM2-ES, IPSL-CM5A-RL, and MIROC5 for the pre-industrial control (PiControl) scenario from 1976 to 2099, historical warming from 1976 to 2005 and three future scenarios (RCP 2.6, 6.0 and 8.5) from 2006 to 2099 for the grid cell overlying Lough Feeagh. The PiControl scenario represents a climate with natural variability under a stable CO_2 concentration of 286 ppm (scenario without anthropogenic climate warming), the historical scenario is based on historical changes in atmospheric CO_2 concentration and RCP 2.6, 6.0 and 8.5 encompass a range of potential future global radiative forcing from anthropogenic greenhouse gases. The RCPs are labelled based on the increase in radiative forcing values relative to PiControl in the year 2099 (2.6, 6, and 8.5 W m^{-2}, respectively; van Vuuren et al, 2011). RCP 2.6 is the more stringent mitigation pathways that is expected to limit the mean global warming to between 0.3 and 1.7 ^{o}C, RCP 6.0 is an intermediate mitigation pathways where global warming is projected to rise between 1.4 and 3.1 ^{o}C and RCP 8.5 is the non-mitigation pathway in which global warming is projected to rise by 2.6 to 4.8 ^{o}C by the late-21st century (IPCC AR5, 2014).

2.4 Model set-up and calibration

Daily climate forcing data from 2004 to 2016 were retrieved from the global gridded data set of historical climatic input (EWEMBI; Lange, 2019). These were the same data that were used to bias correct the ISIMIP GCM-derived scenarios. The variables for running the Simstrat model were wind speed (m s^{-1}) at 10 m, air temperature (^{o}C) at 2 m, the surface incoming short-wave radiation (W m^{-2}),

vapor pressure (mbar) at 2 m, the surface incoming long-wave radiation (W m^{-2}) and precipitation rate (mm h^{-1}). Vapor pressure was estimated from air pressure and specific humidity according to Leppäranta (2015). Following the ISIMIP Lake Sector protocol, inflows and outflows were not included and we assumed a fixed water level, and the sediment heat flux was set to 0 W m^{-2} (Golub et al., 2022). The initial water temperature profile was derived from in situ measurements. Simstrat was run with a timestep of 600 s and the simulated water temperature profiles were saved every hour at 0.5 m depth intervals so that each vertical profile contained a total of 94 layers.

Model parameters were set to default values and three of them were calibrated (Supl. 1). The calibrated parameters p_radin and f_wind scale the incoming short-wave radiation and the wind speed respectively and the parameter a_seiche determines the fraction of wind energy that is transferred to internal seiches. The calibration was performed using PEST (model-independent Parameter ESTimation and uncertainty analysis: https://pesthomepage.org/) software. For the calibration, hourly water temperatures from simulations forced using daily meteorological forcing data were compared with hourly average measured water temperature (Figure S1.1 and S1.2). The hourly average water temperature profiles were derived from high-frequency water temperature measurements collected at the deepest point of the lake every 2 min for the period 2004-2016 at depths of 0.9, 2.5, 5, 8, 11, 14, 16, 18, 20, 22, 27, 32 and 42 m using submerged platinum resistance thermometers (PRTs: Labfacility PT100 1/10DIN 4 wire sensor, www.labfacility.co.uk, Bognor Regis, UK) (de Eyto et al., 2020).

2.5 Heat budget

The heat content variation in the water column, ΔU_{total}, is the sum of the energy fluxes into the lake and includes net surface heat flux, advective heat transport and geothermal heat flux. In this study, the advective and geothermal heat fluxes were set to zero, so the heat content variation is computed by considering only the net surface heat flux Q_{total}. The heat content variation in the water column ΔU_{total} (J m^{-2}) from t-1 to time t can be quantified by:

$$\Delta U_{total} = \frac{1}{A_0}\int_0^{z_{max}} C_w \cdot \rho[z,t] \cdot T[z,t] \cdot \, dV - \frac{1}{A_0}\int_0^{z_{max}} C_w \cdot \rho[z,t-1] \cdot T[z,t-1] \cdot dV = \int_{t-1}^{t} Q_{total} \cdot dt \quad (1)$$

where A_0 is the lake surface area, C_w is the specific heat capacity of water (C_w=4182 J kg^{-1} K^{-1}), ρ[z,t] and T[z,t] represent water density (kg m^{-3}) and temperature (°C), respectively, at time t from lake surface (z=0 m) to bottom (z=z_{max} m) and dV (m^{-3}) is the volume of each water layer, which decreases with depth according to the lake hypsography.

The net or total surface heat flux Q_{total} (W m^{-2}), is computed as the sum of radiative fluxes and turbulent heat fluxes:

$$Q_{total} = Q_{snet} + Q_{lin} + Q_{lout} + Q_e + Q_h \quad (2)$$

Each of the components in Eq. 2 are positive when the lake gains energy (incoming long-wave radiation Q_{lin}, net short-wave radiation Q_{snet}, sensible heat flux Q_h or latent heat flux Q_e) and negative when the lake loses energy (outgoing long -wave radiation Q_{lout}, Q_h or Q_e).

A summary of the heat flux parameterizations for calculating Q_{total} are provided in Table 1. In the Simstrat model 35 % of Q_{sin}, the near-infrared portion of the short-wave radiation, is absorbed directly at the surface. The remaining part, that is 65%, in the visible and ultraviolet portion of the solar radiation spectrum, penetrates through the lake water column and is absorbed according to the Beer-Lambert law:

$$Q_{snet}[z > 0] = (1 - \alpha) \cdot (1 - 0.35) \cdot Q_{sin} \cdot e^{(-K_d \cdot z)} \quad (3)$$

where α is the water albedo (α=0.08), Q_{sin} is the incoming short-wave radiation (W m^{-2}), K_d is the light extinction coefficient (K_d=0.98 m^{-1}) and z (m) is the water depth.

In Simstrat (v2.1.2) the water column is divided into volumes with an area A_{i+1} at the top and A_i at the bottom of the volume and a thickness $h_{i,i+1}$. For this study the code was amended to account for the influence of difference in area between top and bottom of the volume for computation of the short-wave radiation absorption in each layer (Supl. 2). In this amended version the short-wave radiation absorbed by each layer was calculated as:

$$\frac{Q_{snet,i+1} \cdot A_{i+1} - Q_{snet,i} \cdot A_i}{\frac{A_{i+1} + A_i}{2} \cdot h_{i,i+1}} \quad (4)$$

2.6 Data analysis

To assess the impacts of climate change on the surface heat budget components, the PiControl scenario from 1976 to 2099 was compared with scenarios of the same duration that were created by combining the historical scenario from 1976 to 2005 and future GHG emission scenarios (RCP 2.6, 6.0 and 8.5) from 2006 to 2099. The surface heat fluxes (Q_{total}, Q_{snet}, Q_{lin}, Q_{lout}, Q_e and Q_h), volume-weighted average lake temperature T_{avg} and volume-weighted average lake temperature change ΔT_{avg} were derived on a daily basis from the average of hourly simulated outputs. Volume-weighted average lake temperature T_{avg} was estimated from lake temperature profiles and the lake hypsograph curve. In order to distinguish the variations in each of the surface heat budget components for a given season, the data were divided into four distinct temporal databases. Winter was considered to be from December to February, spring from March to May, summer from June to August, and autumn from September to November.

Analysis of long-term and seasonal trends were performed using Generalized Least Squares GLS regression according to Zuur et al. (2007). The effects of temporal autocorrelation were investigated using the auto-correlation function ACF and the partial auto-correlation function PACF. When temporal autocorrelation was detected, a correlation structure using an auto-regressive moving average ARMA(p,q) model for the residuals was included in the model. In order to find the optimal model in terms of the residual correlation structure, the model was applied with different values of p and q. We tried each combination of p = 0, 1, 2 and q = 0, 1, 2. The selected model was the one with the lowest AIC (Akaike information criterion; Akaike, 1987) and the simplest residual correlation structure. Normality and homogeneity assumptions of the residuals were also validated via visual inspection of the histogram of the residuals and the residual-fitted plot respectively. The statistical analysis was carried out using R version 4.0.2 (R Core Team, 2020).

3. Results

3.1. Lake model performance

Simulated water temperatures revealed a good correspondence with observed water temperatures and were reproduced with a high level of accuracy (RMSE=0.79 ^{o}C, NSE=0.95 and BIAS=-0.01 ^{o}C; Supl. 1). The lake model performance was comparable to other studies in Lough Feeagh (RMSE ranged from 0.44 to 0.77 ^{o}C, e.g. Mesman et al., 2020; Bruce et al., 2018).

3.2. Net surface heat budgets

The heat gain by Lough Feeagh over the duration of the future GHG emission scenarios from 1976 to 2099 for the ensemble was, on average, 0.0066 W m^{-2}, 0.0150 W m^{-2} and 0.0429 W m^{-2} for RCP 2.6, 6.0 and 8.5 respectively (Figure 1A). These small imbalances in the long-term surface heat flux led to equivalent ΔT_{avg} increases of 0.64, 1.16 and 2.75 ^{o}C over this 124-year period (or a statistically significant increase rate of T_{avg} 0.05, 0.12, 0.18 ^{o}C decade^{-1}, respectively for RCP 2.6, 6.0 and 8.5). In contrast, under PiControl heat outputs exceeded heat inputs resulting in an average rate of heat loss of -0.0061 W m^{-2} (Figure 1A), that is, a decrease in ΔT_{avg} of 0.12 ^{o}C. It can be seen that the difference between heat inputs and outputs that account for the heat gain or heat loss over the period of 124 years was very small in each scenario.

Long-term annual average Q_{total} from 1976 to 2099 over PiControl and the future GHG emission scenarios showed a high inter-annual variability (Figures 1B-C). Lower standard deviation was found for the future GHG emission scenarios (1.04, 1.02 and 1.01 W m^{-2} for RCP 2.6, 6.0 and 8.5) than for PiControl (1.11 W m^{-2}).

3.3. Turbulent heat and radiative surface fluxes

Net radiation is dominated by the net short-wave radiation budget, Q_{snet}, as incoming and outgoing long-wave fluxes, Q_{lin} and Q_{lout}, are large but opposite in direction, leading to a relatively small net long-wave radiation loss. The combined sensible, Q_h, and latent, Q_e, heat fluxes produced a net surface heat loss. Most of the net radiation is balanced by the turbulent heat loss. Thus, even though there were large changes in the individual heat flux components (Figure 2; Table 2) it is a small imbalance between the turbulent and radiative fluxes that leads to a net lake heat gain or heat loss.

The turbulent heat and radiative surface fluxes showed no significant changes under PiControl over time. However, for the scenarios RCP 2.6, 6.0 and 8.5 significant changes were projected for the individual heat flux components, primarily for Q_e, Q_{lin} and Q_{lout}. The linear trends of the annual averages are listed in Table 2.

The annual average of Q_e changed significantly (Figure 2B), the heat loss increased by 0.34, 0.44 and 0.54 W m^{-2} decade^{-1} for RCP 2.6, 6.0 and 8.5 respectively (Table 2). This change was primarily due to a significant increase in water vapor pressure deficit, e_s-e_a, (0.04, 0.05, 0.08 mbar decade^{-1} respectively for RCP 2.6, 6.0 and 8.5). The transfer function f_u (Table 1), which decreases non-linearly with wind speed, played a secondary role (Supl. 3). Although a significant decrease in f_u was projected (-0.03, -0.03 and -0.06 W m^{-2} mbar^{-1}decade^{-1} respectively for RCP 2.6, 6.0 and 8.5), its effect was not sufficient to compensate for the increase in e_s-e_a (Supl. 3). The flux of sensible heat, Q_h, was the smallest contribution to the heat balance (Figure 2A, Table 2). The greatest sensible heat loss was projected for

PiControl, it was predicted to be on average slightly lower for RCP 2.6, 6.0 and 8.5 (-14.66±0.52, -14.17±0.62, -13.78±0.51, -14.08±0.49 W m^{-2} respectively for PiControl, RCP 2.6, RCP 6.0 and RCP 8.5; Table 2). The annual mean of Q_h did not change significantly, although f_u was projected to significantly decrease, because the weak effect of f_u on Q_h (Supl. 3). This resulted in the annual average Bowen ratio, B, significantly decreasing under GHG emission scenarios.

Regarding radiative heat fluxes, Q_{snet} and Q_{lin} represent gains in lake heat (Figures 2C and 2E) and Q_{lout} represents loss of lake heat (Figure 2D). Q_{lin} was the greatest contribution of lake heat gain (Table 2) and showed the largest projected changes (where there was a significant increase) under future GHG emission scenarios (0.36, 1.02 and 1.75 W m^{-2} $decade^{-1}$ respectively for RCP 2.6, 6.0 and 8.5; Table 2). However, Q_{snet}, on average, contributed lower heat input under future GHG emissions scenarios than for PiControl (Table 2). Q_{lout} was the greatest contributor to lake heat loss (Table 2) and also showed the largest significant increased rates in heat losses (0.40, 0.87 and 1.35 W m^{-2} $decade^{-1}$ respectively for RCP 2.6, 6.0 and 8.5). Q_{lin} and Q_{lout} were opposite in direction, leading to a net long-wave radiation loss Q_{lnet}. The Q_{lnet} heat loss was predicted to be on average lower for RCP 2.6, 6.0 and 8.5 than for PiControl, with a lower Q_{lnet} heat loss at higher RCP (-38.62±1.42, -36.82±1.39, -36.10±1.50 and -35.47±2.25 W m^{-2} respectively for PiControl, RCP 2.6, RCP 6.0 and RCP 8.5; Table 2). Net long-wave heat loss, Q_{lnet}, is also projected to significantly decrease under RCP 6.0 and 8.5 (0.17 and 0.43 W m^{-2} $decade^{-1}$ respectively).

In summary, for the future GHG emission scenarios there were increases in the radiative fluxes (0.41, 0.44, 0.56 W m^{-2} $decade^{-1}$ respectively for RCP 2.6, 6.0 and 8.5; Table 2) that were largely compensated by increasing turbulent heat loss (-0.41, -0.44, -0.55 W m^{-2} $decade^{-1}$ respectively for RCP 2.6, 6.0 and 8.5; Table 2). Therefore, the heat budget was in a quasi-steady state, despite large but compensating changes in the individual fluxes resulting in a small positive imbalance between radiative and turbulent heat fluxes leading to a significant increase in T_{avg} (0.05, 0.12, 0.18 ^{o}C $decade^{-1}$ respectively for RCP 2.6, 6.0 and 8.5).

3.4. Net seasonal surface heat budgets

Lough Feeagh gains heat ($Q_{total}>0$) during spring and summer and loses heat ($Q_{total}<0$) during autumn and winter. The average heat gain for the ensemble in spring from 1976 to 2099 was lower under future GHG emission scenarios than under PiControl (54.81±3.23, 52.92±3.26, 52.59±3.15 and 50.98±4.11 W m^{-2} respectively for PiControl, RCP 2.6, RCP 6.0 and RCP 8.5; Figure 3; Table 3) and the long-term annual average spring heat gain significantly decreased under RCP 6.0 and 8.5 (Figure 3; Table 4) at a rate of -0.29 W m^{-2} $decade^{-1}$ and -0.67 W m^{-2} $decade^{-1}$ for RCP 6.0 and 8.5 respectively. In autumn, the 1976-2099 average heat loss for the ensemble was also lower under future GHG emission scenarios than under PiControl (-45.56±3.44, -44.31±3.34, -43.03±3.97 and -43.19±4.19 W m^{-2} respectively for PiControl, RCP 2.6, RCP 6.0 and RCP 8.5; Figure 3; Table 3). The long-term annual autumnal heat loss was projected to decrease significantly under RCP 6.0 and 8.5 (0.51 and 0.59 W m^{-2} $decade^{-1}$ for RCP 6.0 and 8.5; Table 4). Only small differences in Q_{total} under PiControl and future GHG emission scenarios were projected in summer and winter and showed no significant trends. The average difference in Q_{total} between RCP 8.5 and PiControl resulted in -3.83 and 3.36 W m^{-2} in spring and autumn, respectively (Figure 4). However, the average difference in Q_{total} between RCP 8.5 and PiControl in winter and

summer was an order of magnitude smaller than in spring and autumn (0.41 and 0.30 W m^{-2} in winter and summer, respectively; Figure 4).

The projected rates of heat gain in spring and heat loss in autumn were strongly influenced by the selected Global Climate Model GCM (Supl. 4). The largest average spring rate of heat gain and autumnal rate of heat loss was projected for HadGEM2-ES and the lowest was for GFDL-ESM2M. While there was a general agreement among the models HadGEM2-ES, IPSL-CM5A-LR and MIROC5 in the direction of change in spring rate of heat gain and autumnal rate of heat loss under RCP 2.6, 6.0 and 8.5 relative to PiControl, GFDL-ESM2M gave projections that were the opposite regarding the heat trends in spring and autumn compared to the other GCMs.

3.5. Seasonal turbulent heat and radiative surface fluxes

Total surface heat flux Q_{total}, as well as the turbulent and radiative fluxes, are seasonally variable (Figure 5). During the late-winter and early mid-spring, Lough Feeagh was gaining net radiation thus absorbing heat that resulted in a rapid increase in T_{avg}. Thereafter turbulent heat fluxes played a much more important role in the heat balance. For example, in the late-spring and early-summer Q_{total} leveled off while net radiation was still rising. T_{avg} still kept rising but less rapidly than earlier. The transition from net warming of Lough Feeagh to net cooling occurred in August and T_{avg} started to drop. During late-summer and early-autumn, both turbulent and radiative fluxes contributed to a similar extent to Q_{total}. As autumn progresses, the contribution of the turbulent flux dominated over the radiative flux. Seasonal turbulent and radiative heat fluxes also changed under future GHG emission scenarios relative to the PiControl scenario (Figures 4-5; Tables 3-4).

The spring turbulent heat loss was projected to be larger under future GHG emission scenarios than PiControl because of both latent, Q_e, and sensible, Q_h, heat loss increase (Table 3). Q_e and Q_h heat losses increased significantly under future GHG emission scenarios (Table 4), and in particular the significant increase in Q_h heat loss responded to a faster increase of lake surface water temperature than the overlying air (Supl. 5) and the significant increase in Q_e heat loss responded to a significant increase in both e_s-e_a and f_u, although e_s-e_a had a stronger effect on Q_e than f_u (Supl. 5). The spring radiative heat input was greater under future GHG emission scenarios than PiControl, primarily because of a significant increase in Q_{lin} under future GHG emission scenarios (Table 4). Q_{snet} was projected to be lower under GHG emission scenarios than PiControl (Table 3) and the differences in Q_{snet} between RCPs and PiControl were projected to be the greatest in spring (Figures 4-5). Regarding the spring radiative heat output Q_{lout} also significantly increased under future GHG emission scenarios (Table 4). These combined effects led to an overall reduction in the spring lake heating (Figures 4-5).

During the summer, each individual surface heat flux component reached its peak and showed the greatest change rates (Tables 3-4, Figure 5). However, the significant increase in the heat gain from the net radiative heat flux (0.83, 0.75 and 0.99 W m^{-2} $decade^{-1}$ for RCP 2.6, RCP 6.0 and RCP 8.5; Table 4) was almost equivalent to absolute trends in turbulent heat loss (-0.85, -0.90 and -0.87 W m^{-2} $decade^{-1}$ respectively for RCP 2.6, 6.0 and 8.5; Table 4) with compensating effects, resulting in a steady Q_{total}.

In autumn, the projected turbulent heat flux did not show significant changes over time for both PiControl and future GHG emission scenarios. Under future GHG emission scenarios the long-term

trends in Q_h and Q_e were similar in magnitude and opposite in direction, canceling each other out (Table 4). Q_h heat loss decreased significantly as a result of a significant decrease in both water-air temperature difference T_w-T_a and f_u, but T_w-T_a had a stronger effect on Q_h than f_u (Supl. 5). On the other hand, latent heat loss Q_e increased significantly in response to a significant increase in e_s-e_a and f_u and both showed strong effect on Q_e (Supl. 5). In contrast to turbulent heat flux, radiative heat flux was projected to increase under future GHG emission scenarios (Table 4), resulting in a significant decrease in the lake heat loss.

Lough Feeagh loses heat during the winter and a negligible long-term trend was projected for both PiControl and future GHG emission scenarios. Both winter Q_h and Q_e heat loss increased, but to a lesser extent than in other seasons (Tables 3-4). The winter net radiative flux was negative (heat loss) owing to Q_{snet} heat gain not counteracting the Q_{lnet} heat loss under PiControl and future GHG emission scenarios (Table 3). However, the heat loss by radiative flux significantly decreased under RCP 6.0 and 8.5 (Table 4).

4. Discussion

Understanding how lakes will respond to a changing climate will be essential for their future management. This includes understanding physical changes related to the energy budget of lakes. This is the first study providing a comprehensive analysis of surface heat budget and individual heat flux components under future climate scenarios in a temperate, deep, dystrophic lake, exemplified by Lough Feeagh. Both the annual average of net radiative flux, Q_{rad}, and turbulent heat flux, Q_{tur}, were projected to increase and decrease (Table 2), respectively, with almost equivalent absolute significant trends under GHG emission scenarios, leading to overall a very small and non-significant increase in the total heat budget, Q_{total} (Table 2). In contrast to the steady state, in which the total heat budget would be zero and the lake temperature remain constant, this very small positive imbalance in the total heat budget (quasi-steady state) was sufficient to lead a significant increase in T_{avg} of 0.05, 0.12, 0.18 ^{o}C decade^{-1} respectively for RCP 2.6, 6.0 and 8.5.

Q_{lin} was the radiative flux with the highest contribution to the lake heat budget (Figure 2C; Table 2) and the annual Q_{lin} was also the radiative flux that showed the greatest changes under future GHG emission scenario. Fink et al. (2014) also noted that Q_{lin} was the radiative flux with the greatest significant increases (2.50 W m^{-2} decade^{-1}) at Lake Constance. Solar radiation in CMIP5 global climate models were projected to increase by 0.39 Wm^{-2} decade^{-1} for the period of 2006–2100 over Europe under RCP 8.5 (Bartók et al., 2017). However, Q_{snet} in Lough Feeagh under RCP 8.5 showed non-significant change over time (Figure 2E; Table 2). GCMs include different schemes for the representations of atmospheric processes, aerosols and also the effect of aerosols on cloudiness, atmospheric chemistry, among others (Bartók et al, 2017). The non-significant change in Q_{snet} under RCP 8.5 in Lough Feeagh could be attributed to non-significant changes in cloudiness or water vapor content in the atmosphere. Observed Q_{snet} at Lake Constance from 1984 to 2011 increased at a rate of 2.10 W m^{-2} decade^{-1} (Fink et al, 2014), coinciding with a brightening period in Europe (3.30 W m^{-2} decade^{-1} over 1985-2005; Wild, 2009) which is also captured in the projected Q_{snet} under GHG emissions scenarios.

The increasing incoming radiative fluxes induced higher surface water temperatures and the warmer surface emitted more long-wave radiation and more evaporation. Fink et al. (2014) found similar trends

in heat loss by Q_{lout} (-2.40 W m^{-2} $decade^{-1}$) and Q_e (-2.70 W m^{-2} $decade^{-1}$) and the Q_e contribution to the lake heat loss increased compared to that of Q_{lout}. However, we found that projected heat loss rates were greater for Q_{lout} than Q_e (Table 2). These differences between the heat loss rates for Q_{lout} and Q_e increase inversely proportional to the increase in Q_{snet}, i.e. an increase in Q_{snet} promotes higher Q_e rates, gaining importance as a heat loss compared to Q_{lout}. Consistent with Schmid et al. (2014) we found that sensible heat loss Q_h is the smallest contributor of total surface heat flux (Figure 2A; Table 2). The relative contributions of Q_h and Q_e to the Bowen ratio, B, was found to significantly change under future GHG emission scenarios by allocating more energy to evaporation rather than sensible heating of the atmosphere.

The increase in heat loss is primarily driven by the increase in surface water temperature, as the greater the surface temperature increase, the greater the long-wave heat loss. However, for turbulent heat fluxes it is more complex, because Q_h and Q_e are dependent on the water-air temperature gradient, T_w-T_a, and water-air vapor pressure gradient, e_s-e_a, respectively, and also on the atmospheric stratification and wind speed (f_u, Table 1). Our findings support the assumptions of previous studies that variations in Q_e can be largely explained by e_s-e_a (Nordbo et al., 2011) or by both wind speed and e_s-e_a (Blanken et al., 2000). Even though in Lough Feeagh the average of f_u for the period 1976-2099 was similar in spring and autumn (Supl. 5), in autumn both e_s-e_a and f_u had a strong effect on Q_e (Supl. 5) indicating that Q_e was controlled jointly by the intensity of turbulent mixing and the water-air vapor pressure gradient, while in spring e_s-e_a had a stronger effect on Q_e than f_u did (Supl. 5), indicating Q_e was being controlled by the water-air vapor pressure gradient.

Sediment and advective heat fluxes also contribute to the lake heat budget, but they are not covered in this study. The heat exchange with the sediment is more important for shallow lakes or littoral areas than for deeper lakes where sediments largely do not receive direct solar heating (de la Fuente, 2014) and for ice-covered lakes where the heat fluxes across the lake surface are limited (Schmid and Read, 2021). The advective heat flux has a larger effect in lakes with shorter residence times and can have a warming or cooling effect on lake water temperature, depending on the seasonal differences between the inflow and lake surface temperature. For example, Olsson et al. (2022) found that advective heat flux can be a warming flux in winter and a cooling flux in summer, and that the magnitude of the advective heat flux is determined by the annual water retention time, with the lower the advective heat flux the longer the annual water retention time.

This study showed the counter-intuitive results that, in a warming world where lakes experience warmer water temperatures throughout the year and are projected to continue to warm until the end of the 21st century, there will be less heat entering Lough Feeagh during spring and little change in net heating over the summer compared to natural climate conditions where lake water temperature is not projected to increase. In addition, the reduction of heat loss during autumn together with little change in net heat over winter promoted warmer winter temperatures. As winter temperature have increased, lower net heat entering into the lake is needed in spring to form stratification and subsequently increase the surface water temperatures. In addition, changes in wind forcing played an important role in regulating the vertical distribution of heat in the water column, and consequently in the lake stratification and surface water temperatures.

5. Conclusion

In this study, we analysed the significant changes in the surface heat fluxes under different levels of global warming in Lough Feeagh, an ice-free monomictic lake between the years of 1976 to 2099. We found a small but significant increase in the net radiative flux, Q_{rad} (0.41, 0.44, 0.56 W m^{-2} $decade^{-1}$ respectively for RCP 2.6, 6.0 and 8.5), formed by large changes in the individual radiative fluxes, that was largely counteracted by small but significant decreases in the turbulent fluxes, Q_{tur} (-0.41, -0.44, -0.55 W m^{-2} $decade^{-1}$ respectively for RCP 2.6, 6.0 and 8.5). Ultimately, the combined change in the individual fluxes led to a change in the total surface heat flux, Q_{total}, that was extraordinarily small (0.0066, 0.0150 and 0.0429 W m^{-2} respectively for RCP 2.6, 6.0 and 8.5), but sufficient to lead to significant changes in whole lake water temperature, T_{avg} (0.05, 0.12, 0.18 ^{o}C $decade^{-1}$ respectively for RCP 2.6, 6.0 and 8.5), that were in line with changes found by other modelling studies, and also historical observations. The feedbacks between the lake and atmosphere that affect these fluxes are complex, and this study suggests that even a small difference in an individual flux that affects the balance between them and the resulting total surface heat flux may lead to important changes in water temperature over the time scale of climate change.

On a seasonal scale, the largest change in total surface heat fluxes were in spring and autumn. Both spring heating and autumnal cooling significantly decreased under RCPs (spring heating: -0.29 and -0.67 W m^{-2} $decade^{-1}$ respectively for RCP 6.0 and 8.5 and autumnal cooling: -0.51 and -0.59 W m^{-2} $decade^{-1}$ respectively for RCP 6.0 and 8.5), while small differences in total surface heat flux between PiControl and RCPs were projected in winter and summer. This leads to the counter-intuitive results that in a warming world there will be less heat, not more, entering Lough Feeagh during the spring, and the decreased heat loss during autumn is largely responsible for the long-term changes in volume-weighted average lake temperature.

Acknowledgments

We are grateful to ISIMIP for their role in producing, co-ordinating and making available the ISIMIP climate scenarios. We acknowledge the support of the ISIMIP cross-sectoral science team. We also acknowledge funding from the European Union's Horizon 2020 research and innovation programme under the Marie Skłodowska- Curie grant agreement ID: 722518 (MANTEL ITN), the European Union's Horizon 2020 research and innovation programme within the framework of the project SMARTLAGOON under grant agreement ID: 101017861, and the European Union's JPI Climate project WATExR EU (grant 690462) and Swedish FORMAS grant 2017-01738.

Open Research

The Simstrat v2.1.2 code is available at https://github.com/Eawag-AppliedSystemAnalysis/Simstrat. EWEMBI daily climate forcing data for calibration purposes are provided by Lange (2019). High-frequency water temperature measurements also for calibration purposes are provided by de Eyto et al. (2020). Daily bias-corrected climate model projections from ISIMIP2b are available at https://www.isimip.org/gettingstarted/data-access/. Future projections of surface heat budgets, derived figures and tables, and modified code in Simstrat v.2.1.2 are provided by Ayala et al. (2022).

References

Adrian, R., O'Reilly, C. M., Zagarese, H., Baines, S. B., Hessen, D. O., Keller, W., Livingstone, D. M., Sommaruga, R., Straile, D., van Donk, E., Weyhenmeyer, G. A., and Winder, M. (2009). Lakes as sentinels of climate change. *Limnology and oceanography, 54*(6part2), 2283-2297. https://doi.org/10.4319/lo.2009.54.6_part_2.2283

Akaike, H. (1987). Factor analysis and AIC. In *selected papers of hirotugu akaike* (pp. 371-386). Springer, New York, NY.

Andersen, M. R., de Eyto, E., Dillane, M., Poole, R., and Jennings, E. (2020). 13 years of storms: an analysis of the effects of storms on lake physics on the Atlantic fringe of Europe. *Water, 12*(2), 318. https://doi.org/10.3390/w12020318

Ayala, A. I., Moras, S., and Pierson, D. C. (2020). Simulations of future changes in thermal structure of Lake Erken: proof of concept for ISIMIP2b lake sector local simulation strategy, *Hydrology and Earth System Sciences, 24*(6), 3311–3330. https://doi.org/10.5194/hess-24-3311-2020

Ayala, A. I., Mesman, J. P., Jones, I. D., de Eyto, E., Jennings, E. Goyette, S., and Pierson, D. C. (2022). Future projections of surface heat budgets at Lough Feeagh [Data set]. Zennodo. https://doi.org/10.5281/zenodo.7413519

Bartók, B., Wild, M., Folini, D., Lüthi, D., Kotlarski, S., Schär, C., Vauard, R., Jerez, S., and Imecs, Z. (2017). Projected changes in surface solar radiation in CMIP5 global climate models and in EURO-CORDEX regional climate models for Europe. *Climate dynamics, 49*(7), 2665-2683. https://doi.org/10.1007/s00382-016-3471-2

Bastviken, D., Tranvik, L. J., Downing, J. A., Crill, P. M., and Enrich-Prast, A. (2011). Freshwater methane emissions offset the continental carbon sink. *Science, 331*(6013), 50-50. https://doi.org/10.1126/science.1196808

Blanken, P. D., Rouse, W. R., Culf, A. D., Spence, C., Boudreau, L. D., Jasper, J. N., Kochtubajda, B., Schertzer, W. M., Marsh, P., and Verseghy, D. (2000). Eddy covariance measurements of evaporation from Great Slave lake, Northwest Territories, Canada. *Water Resources Research, 36*(4), 1069-1077.

Bruce, L. C., Frassl, M. A., Arhonditsis, G. B., Gal, G., Hamil-ton, D. P., Hanson, P. C., Hetherington, A. L., Melack, J. M.,Read, J. S., Rinke, K., Rigosi, A., Trolle, D., Winslow, L., Adrian, R., Ayala, A. I., Bocaniov, S. A., Boehrer, B., Boon, C.,Brookes, J. D., Bueche, T., Busch, B. D., Copetti, D., Cortés,A., de Eyto, E., Elliott, J. A., Gallina, N., Gilboa, Y., Guyen-non, N., Huang, L., Kerimoglu, O., Lenters, J.D., MacIntyre, S.,Makler-Pick, V., McBride, C. G., Moreira, S., Özkundakci, D.,Pilotti, M., Rueda, F. J., Rusak, J. A., Samal, N. R., Schmid, M.,Shatwell, T., Snorthheim, C., Soulignac, F., Valerio, G., van derLinden, L., Vetter, M., Vinçon-Leite, B., Wang, J., Weber, M.,Wickramaratne, C., Woolway, R. I., Yao, H., and Hipsey, M. R. (2018). A multi-lake comparative analysis of the General Lake Model (GLM): Stress-testing across a global observatory network. *Environmental Modelling & Software, 102,* 274–291. https://doi.org/10.1016/j.envsoft.2017.11.016

de Eyto, E., Jennings, E., Ryder, E., Sparber, K., Dillane, M., Dalton, C.and Poole, R. (2016). Response of a humic lake ecosystem to an extreme precipitation event: Physical, chemical, and biological implications. *Inland Waters 6*(4), 483–498. https://doi.org/10.1080/IW-6.4.875

de Eyto, E., Dillane, M., Moore, T., Wilson, H., Cooney, J., Hughes, P., and Murphy, M., Nixon, P., Sweeney, D. and Poole, R. (2020). Lough Feeagh water temperature profiles, Marine Institute, Ireland. https://doi.org/10.20393/6C4760C2-7392-4347-8555-28BA0DAD0297

de la Fuente, A. (2014). Heat and dissolved oxygen exchanges between the sediment and water column in a shallow salty lagoon. *Journal of Geophysical Research: Biogeosciences, 119*(4), 596-613. https://doi.org/10.1002/2013JG002413

Deng, K., Azorin-Molina, C., Minola, L., Zhang, G., and Chen, D. (2021). Global near-surface wind speed changes over the last decades revealed by reanalysis and CMIP6 model simulations. *Journal of Climate, 34*(6), 2219-2234. https://doi.org/10.1175/JCLI-D-20-0310.1

Fenocchi, A., Rogora, M., Sibilla, S., and Dresti, C. (2017). Relevance of inflows on the thermodynamic structure and on the modeling of a deep subalpine lake (Lake Maggiore, Northern Italy/Southern Switzerland). *Limnologica, 63*, 42-56. https://doi.org/10.1016/j.limno.2017.01.006

Fink, G., Schmid, M., Wahl, B., Wolf, T., and Wüest, A. (2014). Heat flux modifications related to climate-induced warming of large European lakes. *Water Resources Research, 50*(3), 2072-2085. https://doi.org/10.1002/2013WR014448

Gaudard, A., Råman Vinnå, L., Bärenbold, F., Schmid, M. and Bouffard, D. (2019). Toward an open access to high-frequency lake modeling and statistics data for scientists and practitioners—the case of Swiss lakes using Simstrat v2.1. *Geoscientific Model Development, 12*(9), 3955–3974. https://doi.org/10.5194/gmd-12-3955-2019

Grant, L., Vanderkelen, I., Gudmundsson, L., Tan, Z., Perroud, M., Stepanenko, V. M., Debolskiy, A. V., Droppers, B., Janssen, A. B. G., Woolway, R. I., Choulga, M., Balsamo, G., Kirillin, G., Schewe, J., Zhao, F., del Valle, I. V., Golub, M., Pierson, D. C., Marcé, R., Seneviratne, S. I., and Thiery, W. (2021). Attribution of global lake systems change to anthropogenic forcing. *Nature Geoscience, 14*(11), 849-854. https://doi.org/10.1038/s41561-021-00833-x

Golub, M., Thiery, W., Marcé, R., Pierson, D., Vanderkelen, I., Mercado-Bettin, D., Woolway, R. I., Grant, L., Jennings, E., Kraemer, B. M., Schewe, J., Zhao, F., Frieler, K., Mengel, M., Bogomolov, V. Y., Bouffard, D., Côté, M., Couture, R.-M., Debolskiy, A. V., Droppers, B., Gal, G., Guo, M., Janssen, A. B. G., Kirillin, G., Ladwig, R., Magee, M., Moore, T., Perroud, M., Piccolroaz, S., Raaman Vinnaa, L., Schmid, M., Shatwell, T., Stepanenko, V. M., Tan, Z., Woodward, B., Yao, H., Adrian, R., Allan, M., Anneville, O., Arvola, L., Atkins, K., Boegman, L., Carey, C., Christianson, K., de Eyto, E., DeGasperi, C., Grechushnikova, M., Hejzlar, J., Joehnk, K., Jones, I. D., Laas, A., Mackay, E. B., Mammarella, I., Markensten, H., McBride, C., Özkundakci, D., Potes, M., Rinke, K., Robertson, D., Rusak, J. A., Salgado, R., van der Linden, L., Verburg, P., Wain, D., Ward, N. K., Wollrab, S., and Zdorovennova, G. (2022). A framework for ensemble modelling of climate change impacts on

lakes worldwide: the ISIMIP Lake Sector. *Geoscientific Model Development, 15*(11), 4597–4623. https://doi.org/10.5194/gmd-15-4597-2022

Goudsmit, G.H., Burchard, H., Peeters, F., and Wüest, A. (2002). Application of k-ε turbulence models to enclosed basins: The role of internal seiches. *Journal of Geophysical Research, 107*(C12), 23-1. https://doi.org/10.1029/2001JC000954

Gronewold, A. D., and Stow, C. A. (2014). Water loss from the Great Lakes. *Science, 343*(6175), 1084-1085. https://doi.org/10.1126/science.1249978

Hipsey, M. R., Bruce, L. C., Boon, C., Busch, B., Carey, C. C., Hamilton, D. P., Hanson, P. C., Read, J. S., de Sousa, E., Weber, M., and Winslow, L. A. (2019). A General Lake Model (GLM 3.0) for linking with high-frequency sensor data from the Global Lake Ecological Observatory Network (GLEON). *Geoscientific Model Development, 12*(1), 473–523. https://doi.org/10.5194/gmd-12-473-2019

Hoke A., Woodhouse J., Zoccarato L., McCarthy V., de Eyto E., Calderó-Pascual M., Geffroy E., Dillane M., Grossart H-P and Jennings E. (2020): Impacts of Extreme Weather Events on Bacterial Community Composition of a Temperate Humic Lake. *Water, 12*(10), 2757. https://doi.org/10.3390/w12102757

Huisman, J., Codd, G.A., Paerl, H.W. et al. (2018). Cyanobacterial blooms. Nature Reviews *Microbiology, 16*(8), 471–483. https://doi.org/10.1038/s41579-018-0040-1

Imboden, D. M. and Wüest, A. (1995). Mixing mechanisms in lakes. In *Physics and chemistry of lakes* (pp. 83-138). Springer, Berlin, Heidelberg.

IPCC (2014). Climate Change 2014: Synthesis Report. Contribution of Working Groups I, II and III to the Fifth Assessment Report of the Intergovernmental Panel on Climate Change [Core Writing Team, R.K. Pachauri and L.A. Meyer (eds.)]. IPCC, Geneva, Switzerland, 151 pp.

Jane, S. F., Hansen, G. J.A., Kraemer, B. M., Leavitt, P. R., Mincer, J.L., North, R. L., Pilla, R. M., Stetler, J. T., Williamson, C.E., Woolway, R. I., Arvola, L., Chandra, S., de Gasperi, C. L., Diemer, L., Dunalska,J., Erina, O., Flaim, G., Grossart, H-P, Hambright, K. D., Hein, C., Hejzlar, J., Janus, L. L., Jenny, J. P., Jones, J. R., Knoll, L. B., Leoni, B., Mackay, E., Matsuzaki, S. I. S., McBride, C., Müller-Navarra, D. C., Paterson, A. M., Pierson, D. C., Rogora, M., Rusak, J. A., Sadro, S., Saulnier-Talbot, E., Schmid, M., Sommaruga, R., Thiery, W., Verburg, P., Weathers, K. C., Weyhenmeyer, G. A., Yokota, K., and Rose, K. (2021). Widespread deoxygenation of temperate lakes. *Nature, 594*(7861), 66-70. https://doi.org/10.1038/s41586-021-03550-y

Jansen, J., Woolway, R. I., Kraemer, B. M., Albergel, C., Bastviken, D., Weyhenmeyer, G. A., Marcé, R., Sharma, S., Sobek, S., Tranvik, L. J., Perroud, M., Golub, M., Moore, T. N., Råman Vinnå, L. R., la Fuente, S., Grant, L, Pierson, D. C., Thiery, W., and Jennings, E. (2022). Global increase in methane production under future warming of lake bottom waters. *Global change biology, 28*(18), 5427-5440. https://doi.org/10.1111/gcb.16298

Jeppesen, E., Mehner, T., Winfield, I. J., Kangur, K., Sarvala, J., Gerdeaux, D., Rask, M., Malmquist, H. J., Holmgren, K., Volta, P., Romo, S., Eckmann, R., Sandström, A., Blanco, S., Kangur, A., Ragnarsson Stabo, H., Tarvainen, M., Venteläa, A. M., Søndergaard, M., Lauridsen, T. L., and Meerhoff, M.

(2012). Impacts of climate warming on the long-term dynamics of key fish species in 24 European lakes. *Hydrobiologia, 694*(1), 1-39. https://doi.org/10.1007/s10750-012-1182-1

Kraemer, B. M., Anneville, O., Chandra, S., Dix, M., Kuusisto, E., Livingstone, D. M., Rimmer, A., Schladow, S. G., Silow, E., Sitoki, L. M., Tamatamah, R., Vadeboncoeur, Y., and McIntyre, P. B. (2015). Morphometry and average temperature affect lake stratification responses to climate change. *Geophysical Research Letters, 42*(12), 4981–4988. https://doi.org/10.1002/2015GL064097

La Fuente, S., Jennings, E., Gal, G., Kirillin, G., Shatwell, T., Ladwig, R., Moore, T., Couture R. M., Côté, M., Råman Vinnå, C. L., and Woolway, R. I. (2022). Multi-model projections of future evaporation in a sub-tropical lake. *Journal of Hydrology*, 128729. https://doi.org/10.1016/j.jhydrol.2022.128729

Lange S. (2019). EartH2Observe, WFDEI and ERA-Interim data Merged and Bias-corrected for ISIMIP (EWEMBI). V.1.1. GFZ Data Services. https://doi.org/10.5880/pik.2019.004

Leppäranta, M. (2015). Freezing of lakes. In *Freezing of Lakes and the Evolution of their Ice Cover* (pp. 11-50). Springer, Berlin, Heidelberg.

Li, X., Peng, S., Xi, Y., Woolway, R. I., & Liu, G. (2022). Earlier ice loss accelerates lake warming in the Northern Hemisphere. *Nature communications, 13*(1), 1-9. https://doi.org/10.1038/s41467-022-32830-y

Livingstone, D. M., and Imboden, D. M. (1989). Annual heat balance and equilibrium temperature of Lake Aegeri, Switzerland. *Aquatic Sciences, 51*(4), 351-369. https://doi.org/10.1007/BF00877177

Martin, J. and McCutcheon, M. (1999). Hydrodynamics and Transport for Water Quality Modelling, Lewis Publishers, New York, USA.

Mesman, J. P., Ayala, A. I., Adrian, R., de Eyto, E., Frassl, M. A., Goyette, S., Kasparin, J., Perroud, M., Stelzer, J. A. A., Pierson, D. C. and Ibelings, B. W. (2020). Performance of one-dimensional hydrodynamic lake models during short-term extreme weather events. *Environmental Modelling and Software, 133*, 104852. https://doi.org/10.1016/j.envsoft.2020.104852

Mi, C., Shatwell, T., Ma, J., Xu, Y., Su, F., and Rinke, K. (2020). Ensemble warming projections in Germany's largest drinking water reservoir and potential adaptation strategies. *Science of The Total Environment, 748*, 141366. https://doi.org/10.1016/j.scitotenv.2020.141366

Nordbo, A., Launiainen, S., Mammarella, I., Leppäranta, M., Huotari, J., Ojala, A., and Vesala, T. (2011). Long-term energy flux measurements and energy balance over a small boreal lake using eddy covariance technique. *Journal of Geophysical Research: Atmospheres, 116*(D2). https://doi.org/10.1029/2010JD014542

North, R. P., North, R. L., Livingstone, D. M., Köster, O., and Kipfer, R. (2014). Long-term changes in hypoxia and soluble reactive phosphorus in the hypolimnion of a large temperate lake: consequences of a climate regime shift. *Global change biology, 20*(3), 811-823. https://doi.org/10.1111/gcb.12371

Okoniewska, M., and Szumińska, D. (2020). Changes in potential evaporation in the years 1952–2018 in North-Western Poland in terms of the impact of climatic changes on hydrological and hydrochemical conditions. *Water, 12*(3), 877. https://doi.org/10.3390/w12030877

Olsson, F., Mackay, E. B., Moore, T., Barker, P., Davies, S., Hall, R., Spears, B., Wilkinson, J., and Jones, I. D. (2022). Annual water residence time effects on thermal structure: A potential lake restoration measure? *Journal of environmental management, 314*, 115082. https://doi.org/10.1016/j.jenvman.2022.115082

O'Reilly, C., Sharma, S., Gray, D. K., Hampton, S. E., Read, J. S., Rowle,y R. J., Schneider, P., Lenters, J. D., McIntyre, P.B., Kraemer, B. M., Weyhenmeyer, G. A., Straile, D., Dong, B., Adrian, R., Allan, M. G., Anneville, O., Arvola, L., Austin, J., Bailey, J. L., Baron, J. S., Brookes, J. D., de Eyto, E., Dokulil, M. T., Hamilton, D. P., Havens, K., Hetherington, A. L., Higgins, S. N., Hook, S., Izmest'eva, L. R., Joehnk, K. D., Kangur, K., Kasprzal, P., Kumagai, M., Kuusisto, E., Leshkevich, 20 G., Livingtone, D. M., McIntyre, S., May, L., Melack, J. M., Mueller-Navarra, D. C, Naumenko, M., Noges, P., Noges, T., North, R. P., Plisnier, P. D., Rigosi, A., Rimmer, A., Rogora, M., Rudstam, L. G., Rusak, J. A., Salmaso, N., Samal, N. R., Schindler, D. E., Schladow, S. G., Schmid, M., Schmidt, S. R., Silow, E., Soylu, M. E., Teubner, K., Verburg, P., Voutilainen, A., Watkinson, A., Wiliamson, C. E., and Zhang G. (2015). Rapid and highly variable warming of lake surface waters around the globe. *Geophysical Research Letters, 42*(24), 10773–10781. https://doi.org/10.1002/2015GL066235

Peel, M. C., Finlayson, B. L., and McMahon, T. A. (2007). Updated world map of the Köppen-Geiger climate classification. *Hydrology and earth system sciences, 11*(5), 1633-1644. https://doi.org/10.5194/hess-11-1633-2007

Pekel, J. F., Cottam, A., Gorelick, N., and Belward, A. S. (2016). High-resolution mapping of global surface water and its long-term changes. *Nature, 540*(7633), 418-422. https://doi.org/10.1038/nature20584

Perroud, M., Goyette, S., Martynov, A., Beniston, M. and Anneville, O. (2009). Simulation of multiannual thermal profiles in deep Lake Geneva: A comparison of one-dimensional lake models. *Limnology and oceanography, 54*(5), 1574–1594. https://doi.org/10.4319/lo.2009.54.5.1574

R Core Team (2020). R: A language and environment for statistical computing. R Foundation for Statistical Computing. Vienna, Austria. https://www.R-project.org/.

Råman Vinnå, L., Medhaug, I., Schmid, M., and Bouffard, D. (2021). The vulnerability of lakes to climate change along an altitudinal gradient. *Communications Earth and Environment, 2*(1), 1-10. https://doi.org/10.1038/s43247-021-00106-w

Rice, E., Dam, H. G., and Stewart, G. (2015). Impact of climate change on estuarine zooplankton: surface water warming in Long Island Sound is associated with changes in copepod size and community structure. *Estuaries and coasts, 38*(1), 13-23. https://doi.org/10.1007/s12237-014-9770-0

Rinke, K., Keller, P. S., Kong, X., Borchardt, D., and Weitere, M. (2019). Ecosystem services from inland waters and their aquatic ecosystems. In *Atlas of Ecosystem Services* (pp. 191-195). Springer, Cham. https://doi.org/10.1007/978-3-319-96229-0_30

Schmid, M., Hunziker, S., and Wüest, A. (2014). Lake surface temperatures in a changing climate: a global sensitivity analysis. *Climatic change, 124*(1), 301-315. https://doi.org/10.1007/s10584-014-1087-2

Schmid, M., and Read, J. (2021). Heat budget of lakes. *Reference module in earth systems and environmental sciences*. https://doi.org/10.1016/B978-0-12-819166-8.00011-6

Sharma, S., Blagrave, K., Magnuson, J. J., O'Reilly, C. M., Oliver, S., Batt, R. D., Magee, M. R., Straile, D., Weyhenmeyer, G. A., Winslow, L., and Woolway, R. I. (2019). Widespread loss of lake ice around the Northern Hemisphere in a warming world. *Nature Climate Change, 9*(3), 227-231. https://doi.org/10.1038/s41558-018-0393-5

Sharma, S., Richardson, D. C., Woolway, R. I., Imrit, M. A., Bouffard, D., Blagrave, K., Daly, J., Filazzola, A., Granin, N., Korhonen, J., Magnuson, J., Marszelewski, W., Matsuzaki, S., Perry, W., Robertson, D. M., Rudstam, L. G., Weyhenmeyer, G. A., and Yao, H. (2021). Loss of ice cover, shifting phenology, and more extreme events in Northern Hemisphere lakes. *Journal of Geophysical Research: Biogeosciences, 126*(10), e2021JG006348. https://doi.org/10.1029/2021JG006348

Shatwell, T., Thiery, W., and Kirillin, G. (2019). Future projections of temperature and mixing regime of European temperate lakes. *Hydrology and Earth System Sciences, 23*(3), 1533-1551. https://doi.org/10.5194/hess-23-1533-2019

Smith, L. C., Sheng, Y., MacDonald, G. M., and Hinzman, L. D. (2005). Disappearing arctic lakes. *Science, 308*(5727), 1429-1429. https://doi.org/10.1126/science.1108142

Stepanenko, V., Jöhnk, K. D., Machulskaya, E., Perroud, M., Subin, Z., Nordbo, A., Mammarella, I. and Mironov, D. (2016). Simulation of surface energy fluxes and stratification of a small boreal lake by a set of one-dimensional models. *Tellus A: Dynamic Meteorology and Oceanography, 66*(1), 21389. https://doi.org/10.3402/tellusa.v66.21389

Till, A., Rypel, A. L., Bray, A., and Fey, S. M. (2019). Fish die-offs are concurrent with thermal extremes in north temperate lakes. *Nature Climate Change, 9*(8), 637–641. https://doi.org/10.1038/s41558-019-0520-y

Vachon, D., Langenegger, T., Donis, D., and McGinnis, D. F. (2019). Influence of water column stratification and mixing patterns on the fate of methane produced in deep sediments of a small eutrophic lake. *Limnology and Oceanography, 64*(5), 2114-2128. https://doi.org/10.1002/lno.11172

Vanderkelen, I., Van Lipzig, N. P., Lawrence, D. M., Droppers, B., Golub, M., Gosling, S. N., Janssen, A. B. G., Marcé, R., Müller Schmied, H., Perroud, M., Pierson, D., Pokhrel, Y., Satoh, Y., Schewe, J., Seneviratne, S., I., Stepanenko, V. M., Tan, Z., Woolway, R. I., and Thiery, W. (2020). Global heat uptake by inland waters. *Geophysical Research Letters, 47*(12), e2020GL087867. https://doi.org/10.1029/2020GL087867

van Vuuren, D. P., Edmonds, J., Kainuma, M., Riahi, K., Thomson, A., Hibbard, K., Hurtt, G. C., Kram, T., Krey, V., Lamarque, J. F., Masui, T., Meinshausen, M., Nakicenovic, N. and Rose, S. K. (2011). The

representative concentration pathways: an overview. *Climatic change, 109*(1), 5-31. https://doi.org/10.1007/s10584-011-0148-z

Wang, W., Lee, X., Xiao, W., Liu, S., Schultz, N., Wang, Y., Zhang, M., and Zhao, L. (2018). Global lake evaporation accelerated by changes in surface energy allocation in a warmer climate. *Nature Geoscience, 11*(6), 410-414. https://doi.org/10.1038/s41561-018-0114-8

Weinberger, S., and Vetter, M. (2014). Lake heat content and stability variation due to climate change: coupled regional climate model (REMO)-lake model (DYRESM) analysis. *Journal of Limnology, 73*(1). https://doi.org/10.4081/jlimnol.2014.668

Wild, M. (2009). Global dimming and brightening: A review. *Journal of Geophysical Research: Atmospheres, 114*(D10). https://doi.org/10.1029/2008JD011470

Willett, K. M., Gillett, N. P., Jones, P. D., and Thorne, P. W. (2007). Attribution of observed surface humidity changes to human influence. *Nature, 449*(7163), 710-712. https://doi.org/10.1038/nature06207

Woolway, R. I., Jones, I. D., Hamilton, D. P., Maberly, S. C., Muraoka, K., Read, J. S., Smyth, R. L., and Winslow, L. A. (2015). Automated calculation of surface energy fluxes with high-frequency lake buoy data. *Environmental Modelling & Software, 70*, 191-198. https://doi.org/10.1016/j.envsoft.2015.04.013

Woolway, R. I., Verburg, P., Lenters, J. D., Merchant, C. J., Hamilton, D. P., Brookes, J., de Eyto, E., Kelly, S., Healey, N. C., Hook, S., Lass, A., Pierson, D. C., Rusak, J. A., Kuha, J., Karjalainen, J., Kallio, K., Lepistö, A., and Jones, I. D. (2018). Geographic and temporal variations in turbulent heat loss from lakes: A global analysis across 45 lakes. *Limnology and Oceanography, 63*(6), 2436-2449. https://doi.org/10.1002/lno.10950

Woolway, R.I., and Merchant, C.J. (2019). Worldwide alteration of lake mixing regimes in response to climate change. *Nature Geoscience, 12*(4), 271-276. https://doi.org/10.1038/s41561-019-0322-x

Woolway, R.I., Jennings, E., Shatwell, T., Golub, M., Pierson, D. C., and Maberly, S. C. (2021a). Lake heatwaves under climate change. *Nature, 589*(7842), 402–407. https://doi.org/10.1038/s41586-020-03119-1

Woolway, R. I., Sharma, S., Weyhenmeyer, G. A., Debolskiy, A., Golub, M., Mercado-Bettín, D., Perroud, M., Stepanenko, V., Tan, Z., Grant, L., Ladwing, R., Mesman, J., Moore, T. N., Shatwell, T., Vanderkelen, I., Austin, J. A., DeGasperi, C. L, Dokulil, M., la Fuente, S., Mackay, E. B., Schladow, S. G., Watanabe, S., Marcé, R., Pierson, D. C., Thierey, W., and Jennings, E. (2021b). Phenological shifts in lake stratification under climate change. *Nature communications, 12*(1), 1-11. https://doi.org/10.1038/s41467-021-22657-4

Woolway, R. I., Denfeld, B., Tan, Z., Jansen, J., Weyhenmeyer, G. A., and La Fuente, S. (2021c). Winter inverse lake stratification under historic and future climate change. Limnology and Oceanography Letters, https://doi.org/10.1002/lol2.10231.

Woolway, R. I., Albergel, C., Frölicher, T. L., and Perroud, M. (2022). Severe lake heatwaves attributable to human-induced global warming. *Geophysical Research Letters, 49*(4), e2021GL097031. https://doi.org/10.1029/2021GL097031

Zeng, Z., Ziegler, A. D., Searchinger, T., Yang, L., Chen, A., Ju, K., Piao, S., Li, L. Z. Li., Ciais, P., Chen, D., Liu, J., Azorin-Molina, C., Chappell, A., Medvigy, D., and Wood, E. F. (2019). A reversal in global terrestrial stilling and its implications for wind energy production. *Nature Climate Change, 9*(12), 979-985. https://doi.org/10.1038/s41558-019-0622-6

Zhou, W., Wang, L., Li, D., and Leung, L. R. (2021). Spatial pattern of lake evaporation increases under global warming linked to regional hydroclimate change. *Communications Earth & Environment, 2*(1), 1-10. https://doi.org/10.1038/s43247-021-00327-z

Zuur, A. F., Ieno, E. N., and Smith, G. M. (2007). Analysis of ecological data. Statistics for biology and health. Springer. Heidelberg, Germany.

Table 1. Energy flux components at the air-water interface for the ice-free period in Simstrat v2.1.2. The sign convention is defined in the main text.

Model constant	Value	Unit	Remarks
Q_{snet}	$Q_{snet} = (1-\alpha)\cdot Q_{sin}$	W m^{-2}	Net short-wave radiation
Q_{sin}		W m^{-2}	Incoming short-wave radiation
α	0.08	-	Water albedo
Q_{lin}		W m^{-2}	Incoming long-wave radiation
Q_{lout}	$\varepsilon_w \cdot \sigma \cdot T_w^4$	W m^{-2}	Outgoing long-wave radiation
ε_w	0.97	-	Emissivity of the water
σ	5.67 10^{-8}	W m^{-2} K^{-4}	Stefan-Boltzmann constant
T_w		K	Absolute temperature of water surface
Q_e	$-f_u \cdot (e_s - e_a)$	W m^{-2}	Flux of latent heat
f_u	$\left\{\left[2.7\left(\frac{T_w - T_a}{1-0.378\cdot\frac{e_a}{p_a}}\right)^{\frac{1}{3}}\right]^2 + \left(0.6072\cdot 3.1\cdot\sqrt{u_{10}^2+v_{10}^2}\right)^2\right\}^{\frac{1}{2}}$	W m^{-2} K^{-1}	Empirical transfer function
T_a		K	Absolute atmospheric temperature at 2m
e_a		mbar*	Atmospheric water-vapor pressure at 2 m
u_{10}, v_{10}		m s^{-1}	Wind speed at 10 m
p_a		mbar	Surface air pressure
e_s	$[1+10^{-6}\cdot p_a\cdot(4.5+6\cdot10^{-5}\cdot T_w^2)]\cdot 10^{\frac{0.7859+0.03477\cdot T_w}{1+0.00412\cdot T_w}}$	mbar	Saturated water vapor pressure at lake surface temperature
Q_h	$-\gamma\cdot f_u\cdot(T_w - T_a)$	W m^{-2}	Sensible heat flux
γ	0.61	-	Psychrometric constant

*1mbar=1hPa

Table 2. Ensemble mean μ, standard deviation σ and trend analysis of annual average Q_{total}, Q_h, Q_e, Q_{lin}, Q_{lout}, Q_{snet}, Q_{rad} and Q_{tur} (significance: p-value < 0.05) and the average contribution of Q_h, Q_e, Q_{lin}, Q_{lout}, Q_{snet} (Q_{rad}, Q_{tur}) to Q_{total} from 1976 to 2099 (contribution of Q_i to Q_{total} = Q_i / ($|Q_h|+|Q_e|+|Q_{lin}|+|Q_{lout}|+|Q_{snet}|$), where i = h, e, lin, lout, snet (rad, tur)).

		μ [W m^{-2}]*	σ [W m^{-2}]	rate [W m^{-2}dec^{-1}]+	p-value	Contribution to Q_{total} [%]
PiControl	Q_{total}	-0.0061	1.11	-	>0.05	
	Q_h	-14.6639	0.52	-	>0.05	-1.58
	Q_e	-46.1768	0.92	-	>0.05	-5.10
	Q_{lin}	322.4108	1.73	-	>0.05	38.54
	Q_{lout}	-361.0334	1.07	-	>0.05	-43.04
	Q_{snet}	99.4573	2.02	-	>0.05	10.91
	Q_{rad}	60.8347	1.16	-	>0.05	92.49
	Q_{tur}	-60.8408	1.12	-	>0.05	-7.51
RCP 2.6	Q_{total}	0.0066	1.04	-	>0.05	
	Q_h	-14.1654	0.62	-0.0770	<0.05	-1.51
	Q_e	-47.3234	1.64	-0.3430	<0.05	-5.17
	Q_{lin}	328.5099	2.38	0.3259	<0.001	38.84
	Q_{lout}	-365.3291	2.27	-0.4014	<0.001	-43.08
	Q_{snet}	98.3146	2.71	0.4172	<0.05	10.65
	Q_{rad}	61.4954	1.99	0.4134	0.05	92.58
	Q_{tur}	-61.4888	1.95	-0.4146	0.05	-7.42
RCP 6.0	Q_{total}	0.0150	1.02	-	>0.05	
	Q_h	-13.7763	0.51	-	>0.05	-1.46
	Q_e	-47.3965	1.97	-0.4427	<0.001	-5.17
	Q_{lin}	330.4346	3.96	1.0212	<0.001	38.97
	Q_{lout}	-366.5363	3.32	-0.8656	<0.001	-43.12
	Q_{snet}	97.2895	2.45	0.2661	<0.001	10.52
	Q_{rad}	61.1878	1.99	0.4402	<0.001	92.62
	Q_{tur}	-61.1728	2.08	-0.4438	<0.001	-7.38
RCP 8.5	Q_{total}	0.0429	1.01	-	>0.05	
	Q_h	-14.0848	0.49	-	>0.05	-1.49
	Q_e	-48.0120	2.26	-0.5435	<0.001	-5.20
	Q_{lin}	332.8595	6.67	1.7490	<0.001	39.04
	Q_{lout}	-368.3260	5.03	-1.3460	<0.001	-43.09
	Q_{snet}	97.6062	2.64	-	>0.05	10.49
	Q_{rad}	62.1397	2.37	0.5592	<0.001	92.62
	Q_{tur}	-62.0968	2.41	-0.5536	<0.001	-7.38

*Positive values mean that the lake is gaining heat while negative values mean that the lake is losing heat.

+When the lake is gaining heat and the trend is positive it means that the heat gain is increasing, however if the trend is negative it means that the heat gain is decreasing. When the lake is losing heat and the trend is positive it means that heat loss is decreasing, however if the trend is negative it means that heat loss is increasing.

Table 3. Seasonal mean μ and standard deviation σ of Q_{total}, Q_h, Q_e, Q_{lin}, Q_{lout}, Q_{snet}, Q_{rad} and Q_{tur} from 1976 to 2099 for the ensemble. Positive values mean that the lake is gaining heat while negative values mean that the lake is losing heat.

		Q_{total} [W m^{-2}]		Q_h [W m^{-2}]		Q_e [W m^{-2}]		Q_{lin} [W m^{-2}]		Q_{lout} [W m^{-2}]		Q_{snet} [W m^{-2}]		Q_{rad} [W m^{-2}]		Q_{tur} [W m^{-2}]	
		μ	σ	μ	σ	μ	σ	μ	σ	μ	σ	μ	σ	μ	σ	μ	σ
Spring	PiControl	54.81	3.23	-8.05	1.25	-36.32	1.79	312.35	3.03	-349.84	1.78	136.68	4.53	99.19	2.42	-44.38	2.75
	RCP 2.6	52.92	3.26	-8.11	1.31	-37.18	2.19	318.15	3.02	-353.57	2.44	133.64	4.84	98.21	2.85	-45.29	3.17
	RCP 6.0	52.59	3.15	-7.73	1.25	-37.36	2.49	320.03	3.34	-355.00	3.35	132.65	4.88	97.69	2.83	-45.10	3.44
	RCP 8.5	50.98	4.11	-8.77	1.63	-38.21	2.94	321.86	5.70	-356.46	4.72	132.55	5.46	97.96	3.05	-46.98	4.34
Summer	PiControl	16.40	2.28	-26.52	0.66	-76.52	3.01	348.99	2.64	-396.06	2.50	166.51	6.26	119.44	3.12	-103.04	3.34
	RCP 2.6	16.31	2.57	-25.97	0.94	-78.53	4.18	356.34	3.26	-401.01	3.83	165.48	6.89	120.81	4.63	-104.50	4.86
	RCP 6.0	15.85	2.62	-25.40	0.75	-78.46	4.63	358.26	4.94	-401.86	4.55	163.31	6.49	119.71	4.42	-103.86	4.98
	RCP 8.5	16.70	2.61	-25.50	0.86	-79.26	4.78	361.69	8.24	-404.23	6.46	164.00	6.79	121.46	5.00	-104.76	5.10
Autumn	PiControl	-46.56	3.44	-20.23	1.16	-50.54	1.60	327.35	3.03	-366.07	1.38	62.93	1.95	24.21	1.50	-70.76	2.48
	RCP 2.6	-44.31	3.34	-18.83	0.99	-51.41	1.88	333.74	3.69	-370.81	2.37	63.01	1.97	25.94	1.89	-70.25	2.33
	RCP 6.0	-43.03	3.97	-18.14	1.36	-50.94	2.16	335.60	4.97	-371.93	3.53	62.38	1.94	26.05	2.19	-69.08	2.75
	RCP 8.5	-43.19	4.19	-18.28	1.47	-52.02	2.26	338.22	8.02	-374.10	5.42	62.99	2.26	27.11	2.83	-70.30	2.67
Winter	PiControl	-25.68	5.49	-3.71	2.08	-20.89	1.93	300.58	3.50	-331.64	1.22	29.98	0.91	-1.08	2.20	-24.60	3.74
	RCP 2.6	-25.87	4.46	-3.60	1.68	-21.72	1.80	305.43	3.57	-335.41	1.86	29.43	1.03	-0.55	2.10	-25.32	3.12
	RCP 6.0	-26.33	4.48	-3.68	1.80	-22.38	2.10	307.47	4.31	-336.85	2.90	29.12	1.04	-0.26	1.65	-26.06	3.57
	RCP 8.5	-25.26	4.09	-3.62	1.48	-22.11	1.99	309.27	6.30	-337.99	4.26	29.20	1.04	0.47	2.24	-25.73	3.13

Table 4. Trend analysis of seasonal annual Q_{total}, Q_h, Q_e, Q_{lin}, Q_{lout}, Q_{snet}, Q_{rad} and Q_{tur} from 1976 to 2099 for the ensemble (significance: p-value < 0.05). When the lake is gaining heat and the trend is positive it means that the heat gain is increasing, if the trend is negative it means that the heat gain is decreasing. However, when the lake is losing heat and the trend is positive it means that heat loss is decreasing, if the trend is negative it means that heat loss is increasing.

		Spring		Summer		Autumn		Winter	
		rate [W m^{-2} dec^{-1}]	p-value	rate [W m^{-2} dec^{-1}]	p-value	rate [W m^{-2} dec^{-1}]	p-value	rate [W m^{-2} dec^{-1}]	p-value
Q_{total}	PiControl	-	>0.05	-	>0.05	-	>0.05	-	>0.05
	RCP 2.6	-	>0.05	-	>0.05	-	>0.05	-	>0.05
	RCP 6.0	-0.2915	<0.001	-0.1466	<0.05	0.5116	<0.001	-	>0.05
	RCP 8.5	-0.6661	<0.001	-	>0.05	0.5877	<0.001	-	>0.05
Q_h	PiControl	-	>0.05	-0.0471	<0.05	-	>0.05	-0.1027	0.05
	RCP 2.6	-0.1680	<0.001	-0.1407	<0.001	0.0848	<0.05	-0.0981	<0.05
	RCP 6.0	-0.1647	<0.001	-	>0.05	0.2453	<0.001	-	>0.05
	RCP 8.5	-0.3066	<0.001	-	>0.05	0.2981	<0.001	-0.0880	<0.05
Q_e	PiControl	-	>0.05	-	>0.05	-	>0.05	-0.1069	<0.01
	RCP 2.6	-0.2168	<0.01	-0.7089	<0.001	-0.2056	<0.001	-	>0.05
	RCP 6.0	-0.4487	<0.001	-0.8794	<0.001	-0.2289	<0.001	-0.2062	<0.001
	RCP 8.5	-0.5768	<0.001	-0.9304	<0.001	-0.3219	<0.001	-0.2441	<0.001
Q_{lin}	PiControl	-	>0.05	-	>0.05	-	>0.05	-	>0.05
	RCP 2.6	0.2420	<0.01	0.4975	<0.001	0.4658	<0.001	0.2862	<0.01
	RCP 6.0	0.7129	<0.001	1.2490	<0.001	1.1753	<0.001	0.9605	<0.001
	RCP 8.5	1.3541	<0.001	1.9504	<0.001	1.9647	<0.001	1.5024	<0.001
Q_{lout}	PiControl	-	>0.05	-	>0.05	-	>0.05	-	>0.05
	RCP 2.6	-0.3449	<0.001	-0.6374	<0.001	-0.4138	<0.001	-0.2890	<0.01
	RCP 6.0	-0.8121	<0.001	-1.0498	<0.001	-0.8687	<0.001	-0.7448	<0.001
	RCP 8.5	-1.2007	<0.001	-1.6383	<0.001	-1.4285	<0.001	-1.1178	<0.001
Q_{snet}	PiControl	-	>0.05	-	>0.05	-	>0.05	-	>0.05
	RCP 2.6	0.4386	<0.001	0.9516	<0.001	0.2156	<0.001	0.0838	<0.01
	RCP 6.0	0.4211	<0.001	0.5438	<0.01	0.1165	<0.05	-	>0.05
	RCP 8.5	-	>0.05	-	>0.05	-	>0.05	-	>0.05
Q_{rad}	PiControl	-	>0.05	-	>0.05	-	>0.05	-	>0.05

	RCP 2.6	0.3330	<0.001	0.8264	<0.001	0.2624	<0.001	-	>0.05
	RCP 6.0	0.3219	<0.001	0.7527	<0.001	0.4941	<0.001	0.1858	<0.001
	RCP 8.5	0.2179	<0.01	0.9917	<0.001	0.6826	<0.001	0.3277	<0.001
Q_{tur}	PiControl	-	>0.05	-	>0.05	-	>0.05	-0.2143	<0.01
	RCP 2.6	-0.3860	<0.001	-0.8504	<0.001	-	>0.05	-0.1540	0.05
	RCP 6.0	-0.6134	<0.001	-0.8993	<0.001	-	>0.05	-0.2694	<0.01
	RCP 8.5	-0.8839	<0.001	-0.8705	<0.05	-	>0.05	-0.3321	<0.001

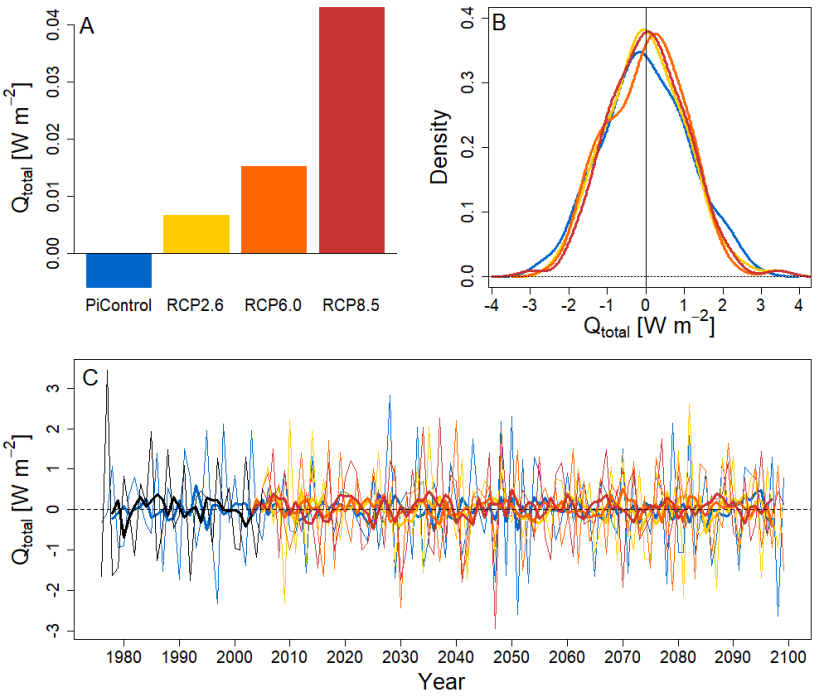

Figure 1. Total surface heat flux, Q_{total}, from 1976 to 2099 under PiControl (blue), historical (black) and future climate forcing: RCP 2.6 (yellow), RCP 6.0 (orange) and RCP 8.5 (red). **A** Average of total surface heat flux over the period 1976 to 2099. **B** Density distribution of annual average total surface heat flux. **C** Annual average total surface heat flux from 1976 to 2099. The thin colored lines show the yearly averages across all GCMs and the thick lines show the 5-year centered moving average of the ensemble.

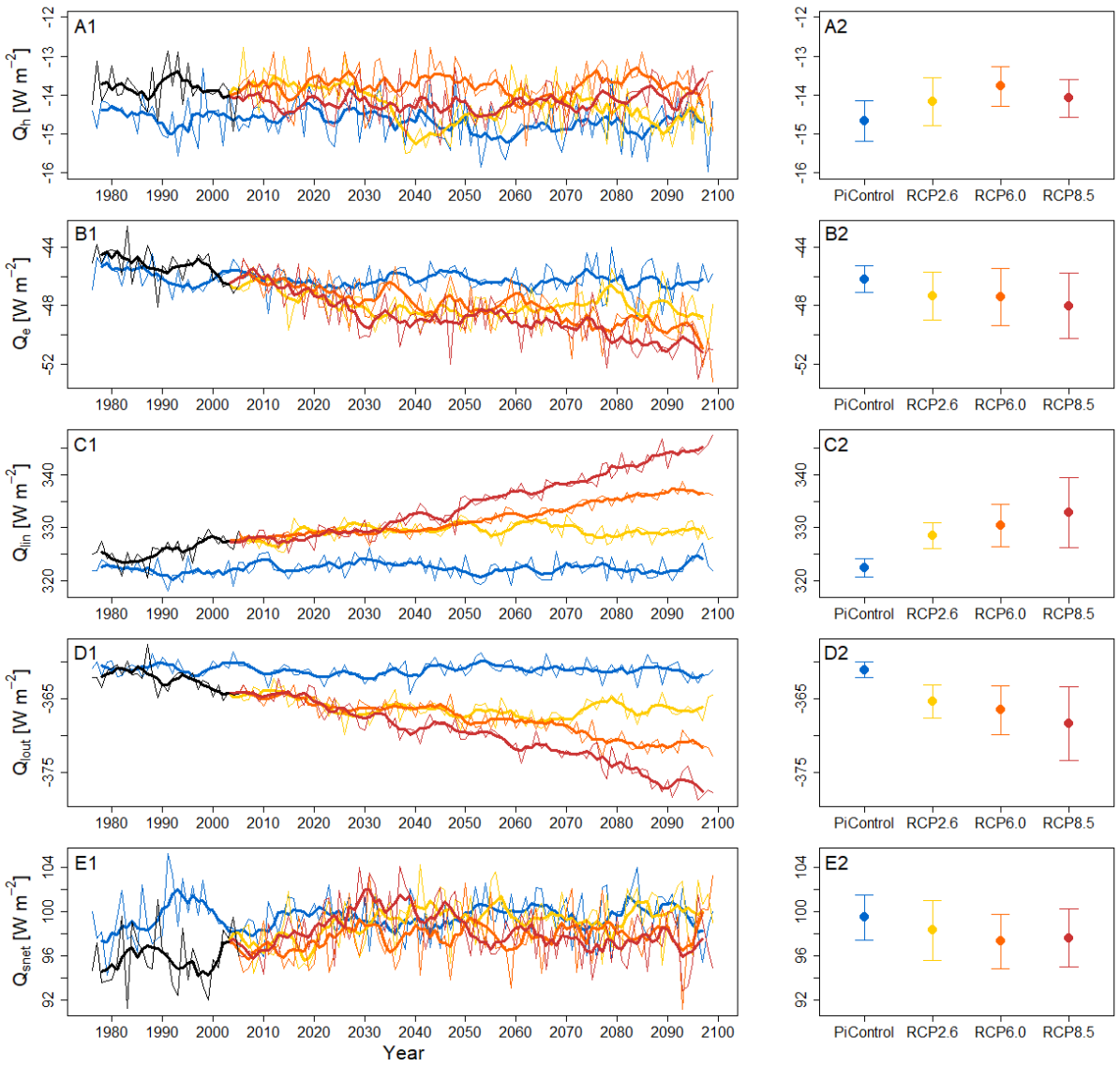

Figure 2. Turbulent heat and radiative surface fluxes. **A** sensible heat flux, Q_h, **B** latent heat flux, Q_e, **C** incoming long-wave radiation, Q_{lin}, **D** outgoing long-wave radiation, Q_{lout}, **E** net short-wave radiation, Q_{snet}, from 1976 to 2099 under PiControl (blue), historic (black) and future climate forcing: RCP 2.6 (yellow), RCP 6.0 (orange) and RCP 8.5 (red). **1** Annual average of each total surface heat flux component, the thin line shows the yearly average across all GCMs and the thick line show the 5-year centered moving average of the ensemble. **2** Average and standard deviation of each total surface heat flux component from 1976 to 2099.

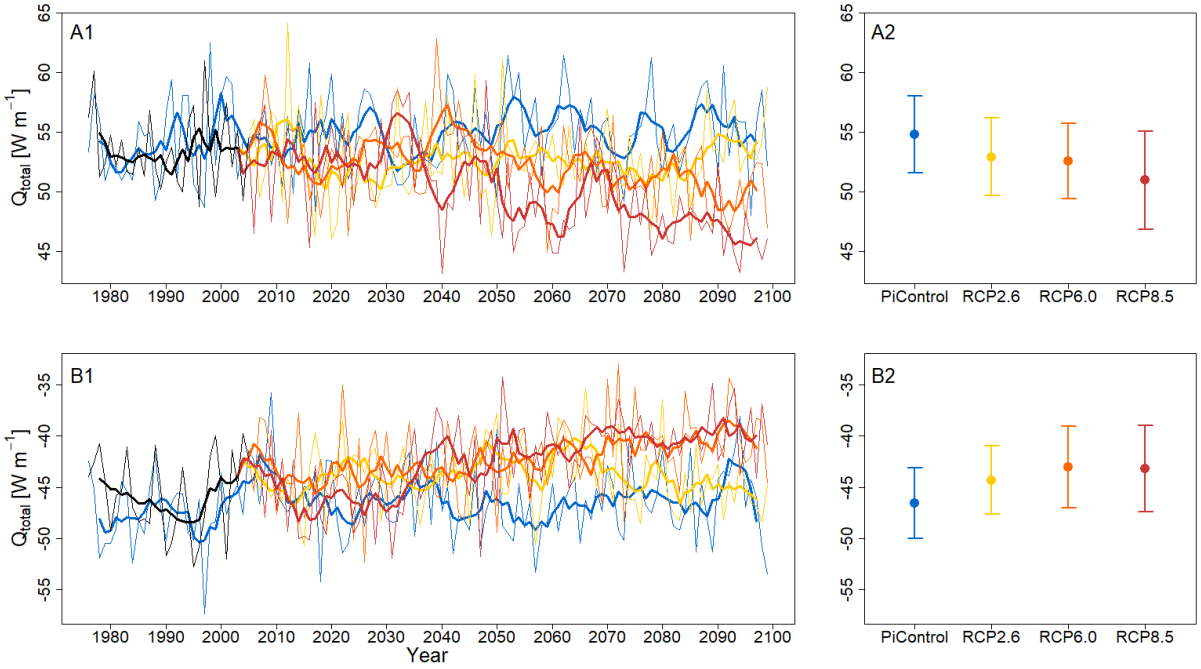

Figure 3. Net seasonal surface heat budgets. **A** Spring and **B** autumn total surface heat flux, Q_{total}, from 1976 to 2099 under PiControl (blue), historic (black) and future climate forcing: RCP 2.6 (yellow), RCP 6.0 (orange) and RCP 8.5 (red). **1** Annual average of total surface heat flux, the thin line shows the yearly average across all GCMs and the thick line show the 5-year centered moving average of the ensemble. **2** Average and standard deviation of total surface heat flux from 1976 to 2099.

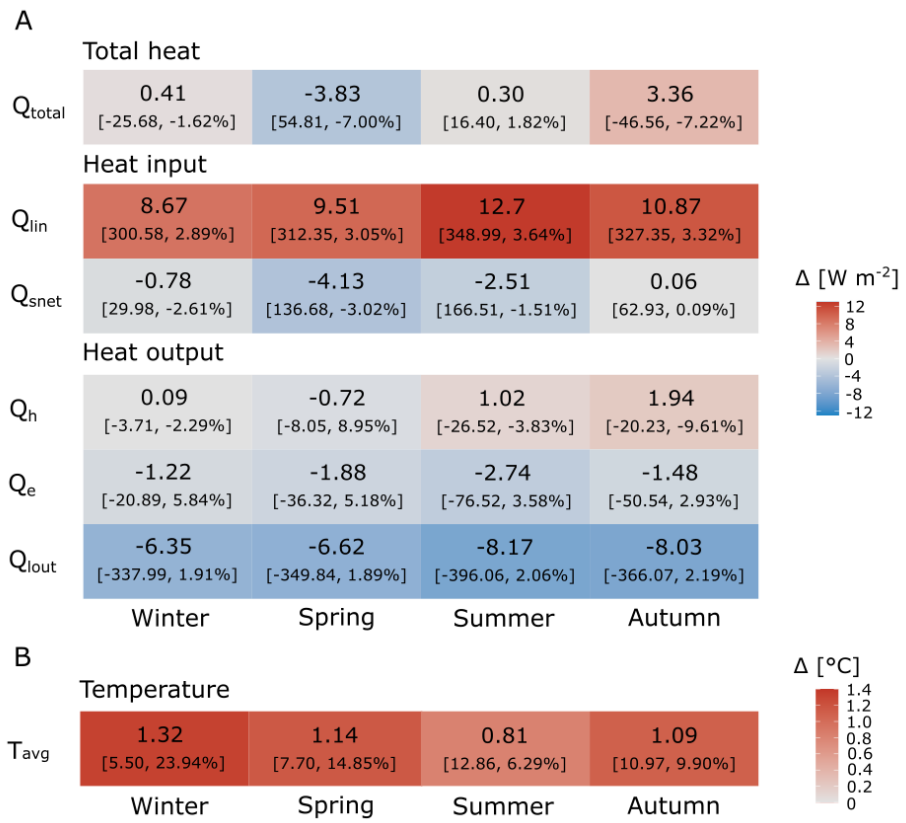

Figure 4. A Seasonal average difference in total surface heat flux, Q_{total}, incoming long-wave radiation, Q_{lin}, net short-wave radiation, Q_{snet}, sensible heat flux, Q_h, latent heat flux, Q_e, and outgoing long-wave radiation, Q_{lout}, between RCP 8.5 and PiControl. **B** Seasonal average difference in volume-weighted average lake temperature, T_{avg}, between RCP 8.5 and PiControl. The two numbers within brackets denote the seasonal average from 1976 to 2099 under PiControl and the seasonal percentage change between RCP 8.5 and PiControl relative to PiControl.

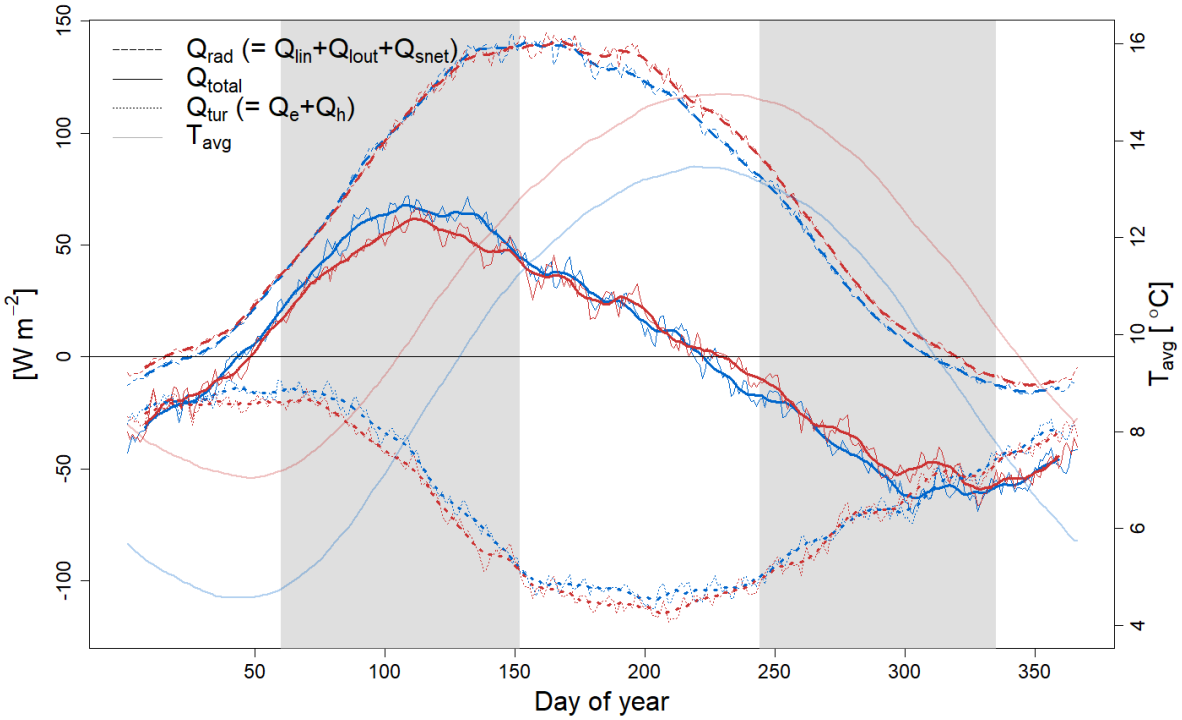

Figure 5. Seasonal total surface heat flux, Q_{total}, turbulent surface heat flux, Q_{tur}, radiative surface heat flux, Q_{rad}, and volume-weighted average lake temperature, T_{avg}, from 2070 to 2099 under PiControl (blue) and RCP 8.5 (red). The thin line shows the daily average across all GCMs and the thick line show the 14-day centered moving average of the ensemble. The shaded areas in the background denote the different seasons (spring: days of the year 60-151, summer: 152-243, autumn: 244-334 and winter: 1-59 and 335-365)**.** The surface heat fluxes are positive when the lake gains heat and negative when the lake loses heat.

Supporting Information for

Climate change impacts on surface heat fluxes in a deep monomictic lake

Ana I. Ayala [1,2], Jorrit P. Mesman[1,2], Ian D. Jones[3], Elvira de Eyto[4], Eleanor Jennings[5], Stéphane Goyette[2], and Donald C. Pierson[1]

[1]Department of Ecology and Genetics/Limnology, Evolutionary Biology Centre, Uppsala University, Uppsala, Sweden.

[2]Institute for Environmental Sciences, University of Geneva, 1205 Geneva, Switzerland.

[3]Biological and Environmental Sciences, Faculty of Natural Sciences, University of Stirling, Stirling, UK.

[4]Marine Institute, Furnace, Newport, Co. Mayo, Ireland.

[5]Centre for Freshwater and Environmental Studies, Dundalk Institute of Technology, Dundalk, Co. Louth, Ireland.

ORCID:

Ana I. Ayala: https://orcid.org/0000-0003-3986-5100

Jorrit P. Mesman: https://orcid.org/0000-0002-4319-260X

Ian D. Jones: https://orcid.org/0000-0002-6898-1429

Elvira de Eyto: https://orcid.org/0000-0003-2281-2491

Eleanor Jennings: https://orcid.org/0000-0001-9828-810X

Stéphane Goyette: https://orcid.org/0000-0001-5199-5974

Donald C. Pierson: https://orcid.org/0000-0001-6230-0146

Corresponding author: Ana I. Ayala (isabel.ayala.zamora@ebc.uu.se)

S1. Lake model calibration

Table S1. Simstrat v2.1.2 parameters.

Parameter	Description and units	Default value	Calibrated value	Calibration range*
lat	Latitude (^{o})	53.94		
p_air	Air pressure (mbar)	995.00 (average)		
a_seiche	Ratio of wind energy going into seiche energy (-)		3.6546e-4	[0.005, 0.0001, 0.05]
q_nn	Fractionation coefficient for seiche energy (-)	1.10		
f_wind	Scaling factor for wind speed (-)		1.0903	[1.00, 0.30, 1.25]
c10	Scaling factor for the wind drag coefficient (-)	1.00		
cd	Bottom drag coefficient (-)	0.002		
hgeo	Geothermal heat flux (W m^{-2})	0.00		
k_min	Minimal value for TKE (J kg^{-1})	1e-9		
p_radin	Scaling factor for the incoming long-wave radiation (-)		1.0504	[1.00, 0.90, 1.10]
p_windf	Scaling factor for the fluxes of sensible and latent heat (-)	1.00		
p_albedo	Scaling factor for snow/ice albedo (-)	1.00		
freez_temp	Water freezing temperature (^{o}C)	0.00		
snow_temp	Temperature below which precipitation fall as snow (^{o}C)	1.00		

*Calibration range: [initial value, lower value, upper value]

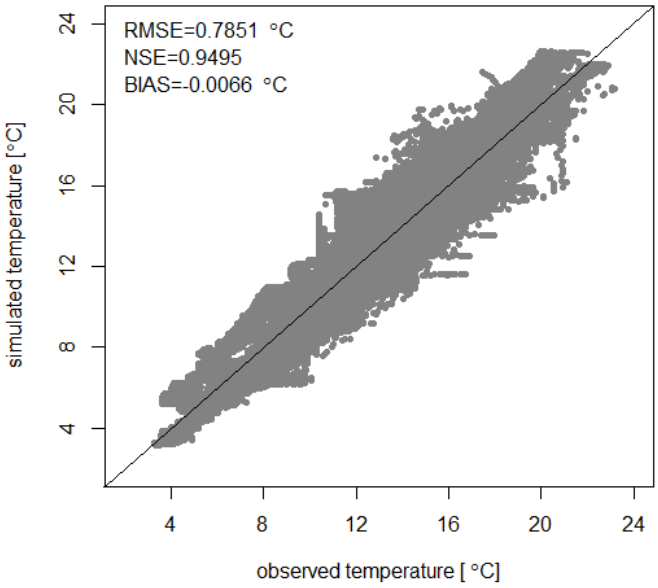

Figure S1.1. Hourly observed vs simulated water temperature from 2004 to 2016.

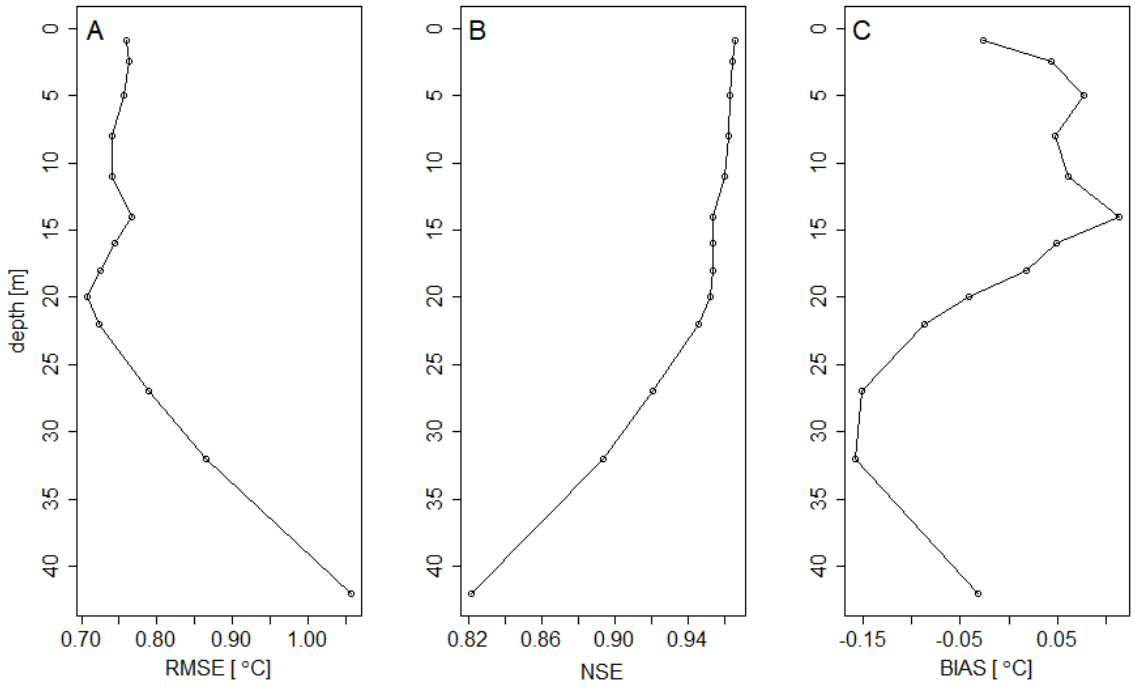

Figure S1.2. Model performance indices at different water depths: A root mean square error, RMSE [^{o}C], B Nash-Sutcliffe efficiency coefficient, NSE, and C mean error, BIAS [^{o}C].

S2. Energy budget for Simstrat v2.1.2 vs modified Simstrat v2.1.2

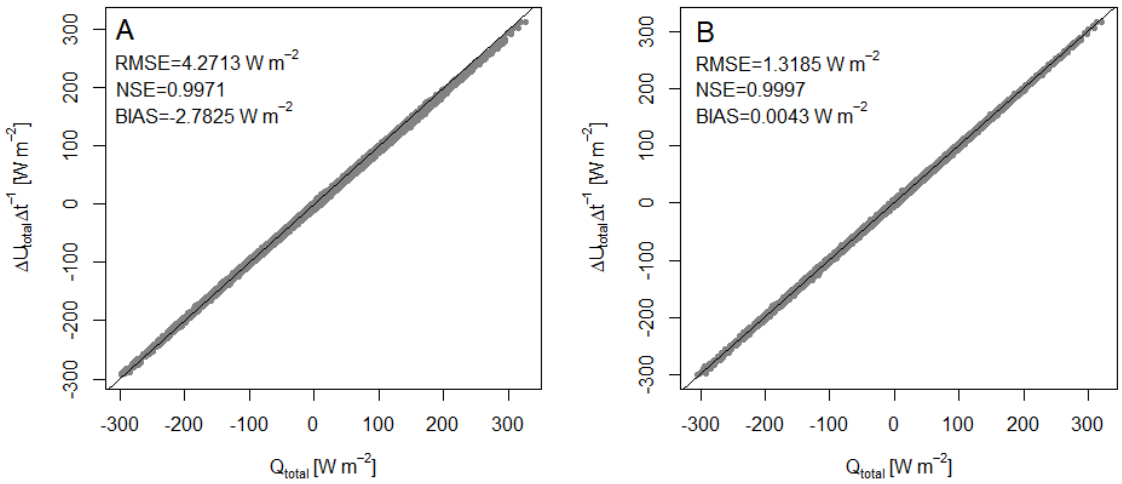

Figure S2.1. Hourly uncalibrated simulations of total surface heat flux, Q_{total}, vs heat content variation, $\Delta U_{total} \Delta t^{-1}$, from 2004 to 2016 for **A** Simstrat v2.1.2 and **B** modified Simstrat v2.1.2.

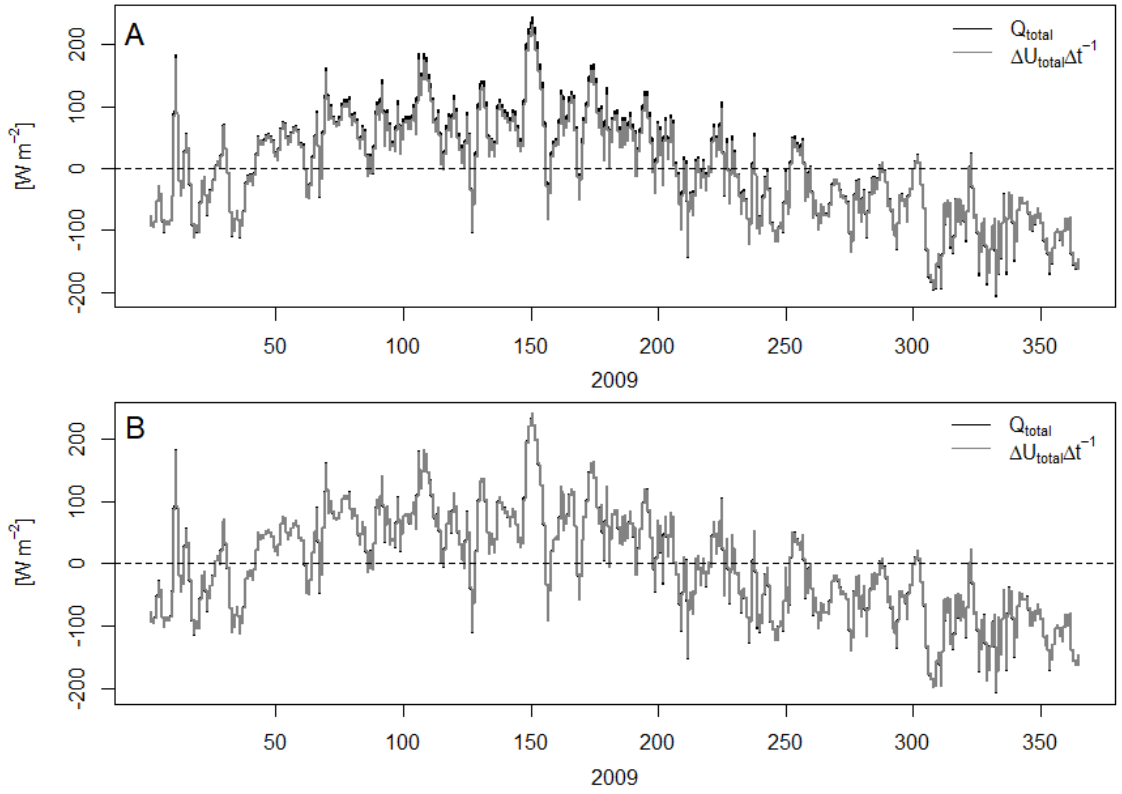

Figure S2.2. Hourly uncalibrated simulations of total surface heat flux, Q_{total}, and heat content variation, $\Delta U_{total} \Delta t^{-1}$, for 2009 for **A** Simstrat v2.1.2 and **B** modified Simstrat v2.1.2.

S3. Q_h and Q_e driving forces

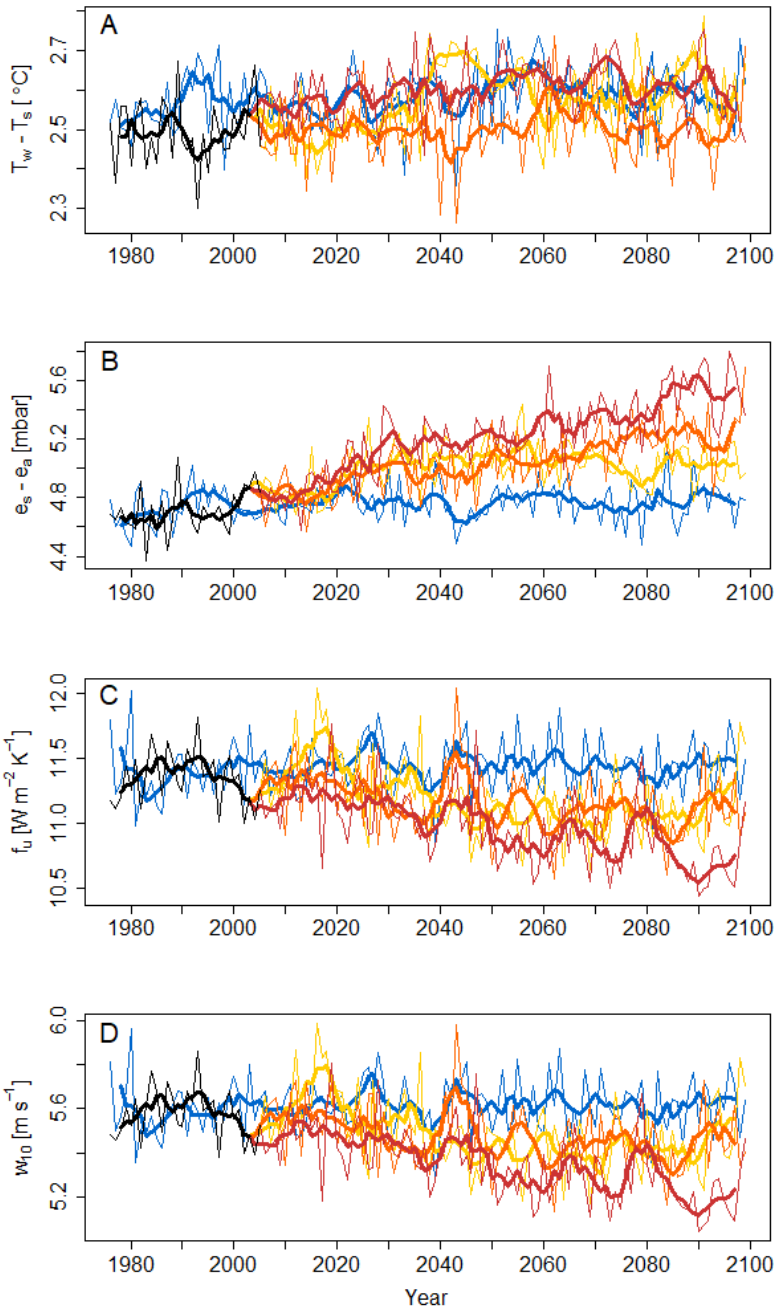

Figure S3.1. Annual average of **A** water-air temperature difference, T_w-T_a, **B** vapor pressure deficit, e_s-e_a, **C** transfer function, f_u, **D** wind speed, w_{10}, from 1976 to 2099 under PiControl (blue), historic (black) and future climate forcing: RCP 2.6 (yellow), RCP 6.0 (orange) and RCP 8.5 (red).

Table S3.1. Ensemble mean, μ, standard deviation, σ, and trend analysis of annual average of T_w-T_a, e_s-e_a, f_u and w_{10} (significance: p-value < 0.05) from 1976 to 2099.

		μ	σ	rate [dec^{-1}]	p-value
PiControl	T_w-T_a [°C]	2.58	0.08		>0.05
	e_s-e_a [mbar]	4.76	0.13		>0.05
	f_u [W m^{-2} K^{-1}]	11.43	0.21		>0.05
	w_{10} [m s^{-1}]	5.61	0.12		>0.05
RCP 2.6	T_w-T_a [°C]	2.55	0.1	0.0123	<0.001
	e_s-e_a [mbar]	4.94	0.2	0.0348	<0.001
	f_u [W m^{-2} K^{-1}]	11.23	0.28	-0.0303	<0.001
	w_{10} [m s^{-1}]	5.51	0.16	-0.0171	<0.001
RCP 6.0	T_w-T_a [°C]	2.5	0.08		>0.05
	e_s-e_a [mbar]	4.97	0.25	0.0541	<0.001
	f_u [W m^{-2} K^{-1}]	11.21	0.25	-0.0303	<0.001
	w_{10} [m s^{-1}]	5.50	0.14	-0.0156	<0.001
RCP 8.5	T_w-T_a [°C]	2.58	0.09	0.0115	<0.001
	e_s-e_a [mbar]	5.1	0.33	0.0805	<0.001
	f_u [W m^{-2} K^{-1}]	11.06	0.31	-0.0596	<0.001
	w_{10} [m s^{-1}]	5.41	0.18	-0.0344	<0.001

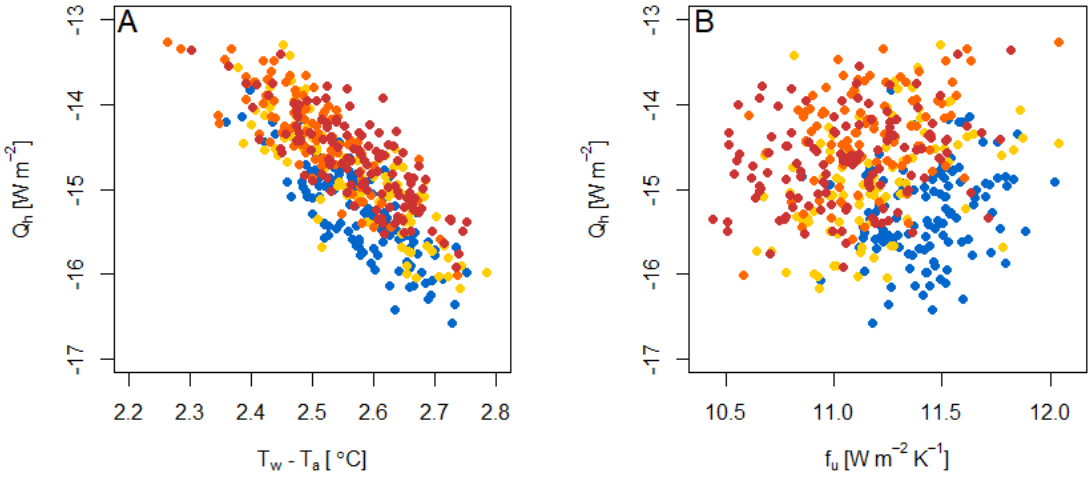

Figure S3.2. A Relationship between annual average water-air temperature difference, T_{water}-T_{atm}, and annual average of sensible heat flux, Q_h. **B** Relationship between annual average of transfer function, f_u, and annual average of sensible heat flux, Q_h. From 1976 to 2099 for PiControl (blue), RCP 2.6 (yellow), RCP 6.0 (orange) and RCP 8.5 (red).

Table S3.2. Summary output from multiple linear regression model used to describe the influence of T_w-T_a and f_u on Q_h. Standardized slope coefficients were calculated to compare the strength of the effect of T_w-T_a and f_u on Q_h. The standardized slope coefficient is measured in units of standard deviation. For example, a β value of 0.6 indicates that a change of 1 standard deviation in the independent variable results in 0.6 standard deviations increase in the dependent variable.

PiControl					
$Q_h \sim T_w$-T_a					
	unstandardized coefficients		standardized coefficients	t	p-value
	B	std error	β		
(constant)	-1.0909	0.99		-1.10	>0.05
T_w-T_a	-5.5004	0.38		-14.33	<0.001
R^2 = 0.6274			R_{adj}^2 = 0.6243		
p-value<0.001					
$Q_h \sim (T_w$-$T_a) + f_u$					
	unstandardized coefficients		standardized coefficients	t	p-value
	B	std error	β		
(constant)	2.3830	2.31		1.03	>0.05
T_w-T_a	-5.7441	0.41	-0.8272	-14.07	<0.001
f_u	-0.2489	0.15	-0.0976	-1.66	>0.05
R^2 = 0.6357			R_{adj}^2 = 0.6297		
p-value<0.001					
RCP 2.6					
$Q_h \sim T_w$-T_a					
	unstandardized coefficients		standardized coefficients	t	p-value
	B	std error	β		
(constant)	-0.5868	0.80		-0.74	>0.05
T_w-T_a	-5.5500	0.31		-17.78	<0.001
R^2 = 0.7216			R_{adj}^2 = 0.7193		
p-value<0.001					
$Q_h \sim (T_w$-$T_a) + f_u$					
	unstandardized coefficients		standardized coefficients	t	p-value
	B	std error	β		
(constant)	5.4852	2.35		2.34	<0.05
T_w-T_a	-6.2195	0.39	-0.9520	-15.95	<0.001
f_u	-0.3884	0.14	-0.1637	-2.74	<0.01
R^2 = 0.7379			R_{adj}^2 = 0.7336		
p-value<0.001					
RCP 6.0					

$Q_h \sim T_w - T_a$					
	unstandardized coefficients		standardized coefficients	t	p-value
	B	std error	β		
(constant)	-0.8900	0.82		-1.09	>0.05
$T_w - T_a$	-5.3900	0.33		-16.48	<0.001
$R^2 = 0.6901$			$R_{adj}^2 = 0.6876$		
p-value<0.001					
$Q_h \sim (T_w - T_a) + f_u$					
	unstandardized coefficients		standardized coefficients	t	p-value
	B	std error	β		
(constant)	2.6536	1.98		1.34	>0.05
$T_w - T_a$	-5.7344	0.37	-0.8837	-15.60	<0.001
f_u	-0.2394	0.12	-0.1114	-1.97	0.05
$R^2 = 0.6997$			$R_{adj}^2 = 0.6947$		
p-value<0.001					
RCP 8.5					
$Q_h \sim T_w - T_a$					
	unstandardized coefficients		standardized coefficients	t	p-value
	B	std error	β		
(constant)	-2.5032	0.82		-2.87	<0.01
$T_w - T_a$	-4.7272	0.33		-13.95	<0.001
$R^2 = 0.6145$			$R_{adj}^2 = 0.6114$		
p-value<0.001					
$Q_h \sim (T_w - T_a) + f_u$					
	unstandardized coefficients		standardized coefficients	t	p-value
	B	std error	β		
(constant)	6.7320	1.90		3.55	<0.001
$T_w - T_a$	-5.9017	0.38	-0.9787	-15.66	<0.001
f_u	-0.5615	0.11	-0.3341	-5.35	<0.001
$R^2 = 0.6682$			$R_{adj}^2 = 0.6831$		
p-value<0.001					

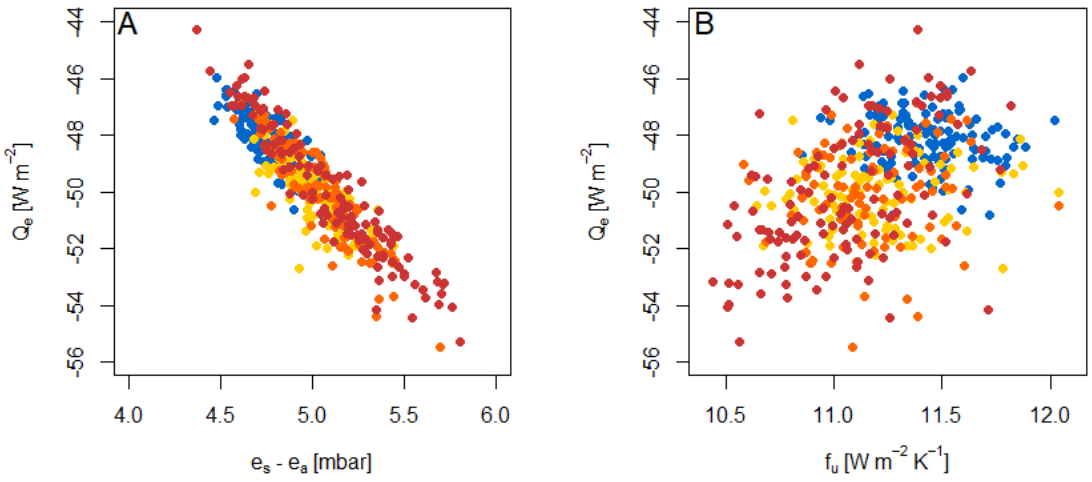

Figure S3.3. A Relationship between annual average of vapor pressure deficit, e_s-e_a, and annual average of latent heat flux, Q_e. **B** Relationship between annual average of transfer function, f_u, and annual average of latent heat flux, Q_e. From 1976 to 2099 for PiControl (blue), RCP 2.6 (yellow), RCP 6.0 (orange) and RCP 8.5 (red).

Table S3.3. Summary output from multiple linear regression model used to describe the influence of e_s-e_a and f_u on Q_e. Standardized slope coefficients were calculated to compare the strength of the effect of e_s-e_a and f_u on Q_e. The standardized slope coefficient is measured in units of standard deviation. For example, a β value of 0.6 indicates that a change of 1 standard deviation in the independent variable results in 0.6 standard deviations increase in the dependent variable.

PiControl					
$Q_e \sim e_s$-e_a					
	unstandardized coefficients		standardized coefficients	t	p-value
	B	std error	β		
(constant)	-21.0932	1.91		-11.04	<0.001
e_s-e_a	-5.6883	0.40		-14.17	<0.001
R^2 = 0.6221			R_{adj}^2 = 0.6190		
p-value<0.001					
$Q_e \sim (e_s$-$e_a) + f_u$					
	unstandardized coefficients		standardized coefficients	t	p-value
	B	std error	β		
(constant)	5.1805	3.03		1.71	>0.05
e_s-e_a	-6.6466	0.32	-0.9216	-21.03	<0.001
f_u	-1.8992	0.19	-0.4304	-9.82	<0.001

R^2 = 0.7897			R_{adj}^2 = 0.7863		
p-value<0.001					
RCP 2.6					
$Q_e \sim e_s\text{-}e_a$					
	unstandardized coefficients		standardized coefficients	t	p-value
	B	std error	β		
(constant)	-13.4119	1.76		-7.63	<0.001
$e_s\text{-}e_a$	-7.2772	0.36		-20.46	<0.001
R^2 = 0.7744			R_{adj}^2 = 0.7725		
p-value<0.001					
$Q_e \sim (e_s\text{-}e_a) + f_u$					
	unstandardized coefficients		standardized coefficients	t	p-value
	B	std error	β		
(constant)	23.8800	3.73		6.40	<0.001
$e_s\text{-}e_a$	-9.1919	0.31	-1.1115	-29.29	<0.001
f_u	-2.4784	0.23	-0.4031	-10.62	<0.001
R^2 = 0.8832			R_{adj}^2 = 0.8813		
p-value<0.001					
RCP 6.0					
$Q_e \sim e_s\text{-}e_a$					
	unstandardized coefficients		standardized coefficients	t	p-value
	B	std error	β		
(constant)	-11.1015	1.33		-2.87	<0.001
$e_s\text{-}e_a$	-7.7155	0.27		-13.95	<0.001
R^2 = 0.8722			R_{adj}^2 = 0.8711		
p-value<0.001					
$Q_e \sim (e_s\text{-}e_a) + f_u$					
	unstandardized coefficients		standardized coefficients	t	p-value
	B	std error	β		
(constant)	22.6908	3.26		6.97	<0.001
$e_s\text{-}e_a$	-9.0691	0.23	-1.0977	-39.70	<0.001
f_u	-2.4144	0.22	-0.2998	-10.85	<0.001
R^2 = 0.9352			R_{adj}^2 = 0.9342		
p-value<0.001					
RCP 8.5					
$Q_e \sim e_s\text{-}e_a$					
	unstandardized coefficients		standardized coefficients	t	p-value
	B	std error	β		
(constant)	-15.4764	0.99		-15.65	<0.001

e_s-e_a	-6.7821	0.19		-35.09	<0.001
R^2 = 0.9098			R_{adj}^2 = 0.9091		
p-value<0.001					
$Q_e \sim (e_s-e_a) + f_u$					
	unstandardized coefficients		standardized coefficients	t	p-value
	B	std error	β		
(constant)	15.9656	3.14		5.09	<0.001
e_s-e_a	-8.2396	0.20	-1.1588	-41.15	<0.001
f_u	-2.1701	0.21	-0.2901	-10.30	<0.001
R^2 = 0.9520			R_{adj}^2 = 0.9512		
p-value<0.001					

Text S3.1. Relationship between sensible heat flux, Q_h, and water-air temperature difference, T_w-T_a, and transfer function, f_u, and also the relationship between latent heat flux, Q_e, and vapor pressure deficit, e_s-e_a, and transfer function, f_u.

T_w-T_a alone explained between 61-72% of the variation in Q_h whereas the addition of f_u to T_w-T_a explained between 64-74%. The standardized slope coefficients for T_w-T_a [-0.98, -0.83] and f_u [-0.33, -0.10] showed that T_w-T_a had a stronger effect on Q_h than f_u and f_u has a weak effect on Q_h. e_s-e_a alone explained between 62-91% of the variation in Q_e whereas the addition of f_u to e_s-e_a explained between 79-95%. The standardized slope coefficients for e_s-e_a [-1.16, -0.92] and f_u [-0.43, -0.29] showed that e_s-e_a had a strong effect on Q_e and f_u has a moderate effect on Q_e.

S4. Seasonal Q_{total}

Table S4.1. Mean, μ, standard deviation, σ, and trend analysis (significance: p-value < 0.05) of seasonal annual average of total surface heat flux Q_{total} from 1976 to 2099 for GFDL-ESM2M, HadGEM2-ES, IPSL-CM5A-LR and MIROC5.

			Q_{total} [W m^{-2}]			
			μ*	σ	rate [dec^{-1}]+	p-value
GFDL-ESM2M	Spring	PiControl	42.95	5.94	-	>0.05
		RCP 2.6	44.24	5.60	-	>0.05
		RCP 6.0	43.77	4.90	-	>0.05
		RCP 8.5	42.22	5.16	-	>0.05
	Autumn	PiControl	-32.33	5.93	-	>0.05
		RCP 2.6	-34.44	5.93	-	>0.05
		RCP 6.0	-33.79	5.24	-	>0.05
		RCP 8.5	-33.74	6.37	0.3406	<0.05
HadGEM2-ES	Spring	PiControl	62.25	7.48	-	>0.05
		RCP 2.6	59.70	8.84	-0.5447	<0.05
		RCP 6.0	59.61	7.49	-0.4640	<0.01
		RCP 8.5	56.88	9.81	-1.1932	<0.001
	Autumn	PiControl	-58.48	8.27	-	>0.05
		RCP 2.6	-54.28	8.31	-	>0.05
		RCP 6.0	-51.86	8.69	0.8314	<0.001
		RCP 8.5	-52.43	8.82	1.0474	<0.001
IPSL-CM5A-LR	Spring	PiControl	60.09	6.81	-	>0.05
		RCP 2.6	59.11	6.50	-	>0.05
		RCP 6.0	58.07	6.95	-0.3676	<0.05
		RCP 8.5	57.90	6.92	-0.7622	<0.001
	Autumn	PiControl	-55.69	7.39	-	>0.05
		RCP 2.6	-53.10	7.37	-	>0.05
		RCP 6.0	-51.09	7.87	0.7336	<0.001
		RCP 8.5	-52.12	7.15	0.6173	<0.001
MIROC5	Spring	PiControl	53.94	6.50	-	>0.05
		RCP 2.6	48.62	6.01	-	>0.05
		RCP 6.0	48.89	6.24	-	>0.05
		RCP 8.5	46.89	5.40	-0.4995	<0.001
	Autumn	PiControl	-39.72	6.01	-	>0.05
		RCP 2.6	-35.32	5.47	-	>0.05
		RCP 6.0	-35.36	6.18	-	>0.05
		RCP 8.5	-34.47	6.19	0.5598	<0.05

*Positive values mean that the lake is gaining heat while negative values mean that the lake is losing heat.

+When the lake is gaining heat and the trend is positive it means that the heat gain is increasing, however if the trend is negative it means that the heat gain is decreasing. When the lake is losing heat

and the trend is positive it means that heat loss is decreasing, however if the trend is negative it means that heat loss is increasing.

S5. Seasonal Q_h and Q_e driving forces

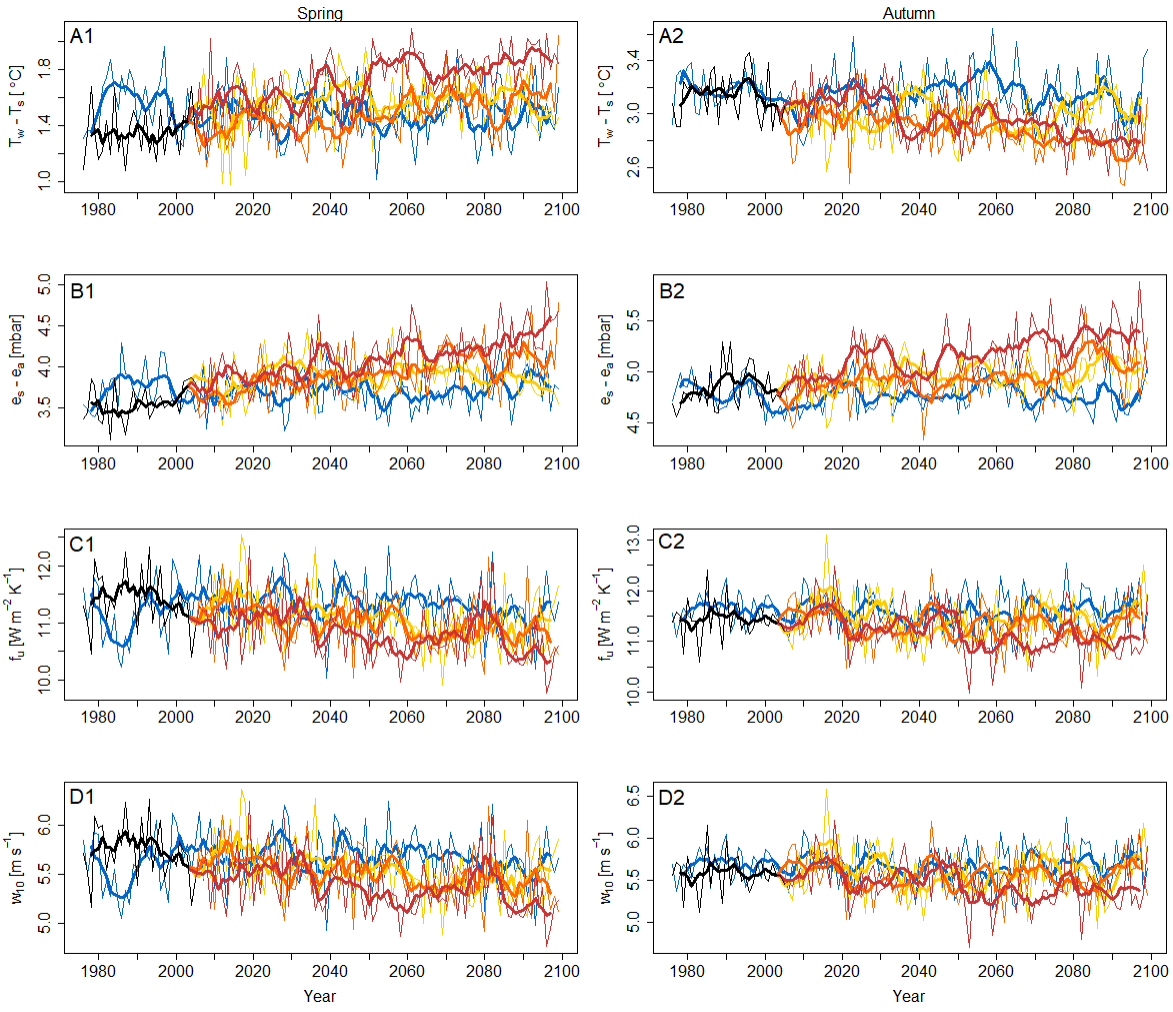

Figure S5.1. Annual average of **A** water-air temperature difference, T_w-T_a, **B** vapor pressure deficit, e_s-e_a, **C** transfer function, fu, **D** wind speed, w_{10}, in **1** spring and **2** autumn from 1976 to 2099 under PiControl (blue), historic (black) and future climate forcing: RCP 2.6 (yellow), RCP 6.0 (orange) and RCP 8.5 (red).

Table S5.1. Ensemble mean, μ, standard deviation, σ, and trend analysis of spring and autumnal annual average of T_w-T_a, e_s-e_a, f_u and w_{10} (significance: p-value < 0.05) from 1976 to 2099.

		Spring				Autumn			
		μ	σ	rate [dec^{-1}]	p-value	μ	σ	rate [dec^{-1}]	p-value
PiControl	T_w-T_a [°C]	1.49	0.19		>0.05	3.16	0.18		>0.05
	e_s-e_a [mbar]	3.71	0.24		>0.05	4.77	0.15		>0.05
	f_u [W m^{-2} K^{-1}]	11.29	0.47		>0.05	11.6	0.39		>0.05
	w_{10} [m s^{-1}]	5.66	0.27		>0.05	5.67	0.23		>0.05
RCP 2.6	T_w-T_a [°C]	1.52	0.20	0.0227	<0.001	3.03	0.18	-0.0118	<0.01
	e_s-e_a [mbar]	3.80	0.27	0.0298	<0.001	4.93	0.20	0.0178	<0.001
	f_u [W m^{-2} K^{-1}]	11.14	0.51	-0.0554	<0.001	11.43	0.45		>0.05
	w_{10} [m s^{-1}]	5.58	0.29	-0.0318	<0.001	5.59	0.27		>0.05
RCP 6.0	T_w-T_a [°C]	1.45	0.2	0.0270	<0.001	2.94	0.21	-0.0348	<0.001
	e_s-e_a [mbar]	3.84	0.33	0.0612	<0.001	4.92	0.23	0.0258	<0.001
	f_u [W m^{-2} K^{-1}]	11.09	0.50	-0.0614	<0.001	11.36	0.38		>0.05
	w_{10} [m s^{-1}]	5.57	0.29	-0.0357	<0.001	5.56	0.23		>0.05
RCP 8.5	T_w-T_a [°C]	1.64	0.25	0.0517	<0.001	3.01	0.20	-0.0327	<0.001
	e_s-e_a [mbar]	3.98	0.38	0.0813	<0.001	5.09	0.28	0.0525	<0.001
	f_u [W m^{-2} K^{-1}]	10.95	0.56	-0.0797	<0.001	11.25	0.45	-0.0459	<0.001
	w_{10} [m s^{-1}]	5.47	0.32	-0.0489	<0.001	5.49	0.26	-0.0232	<0.001

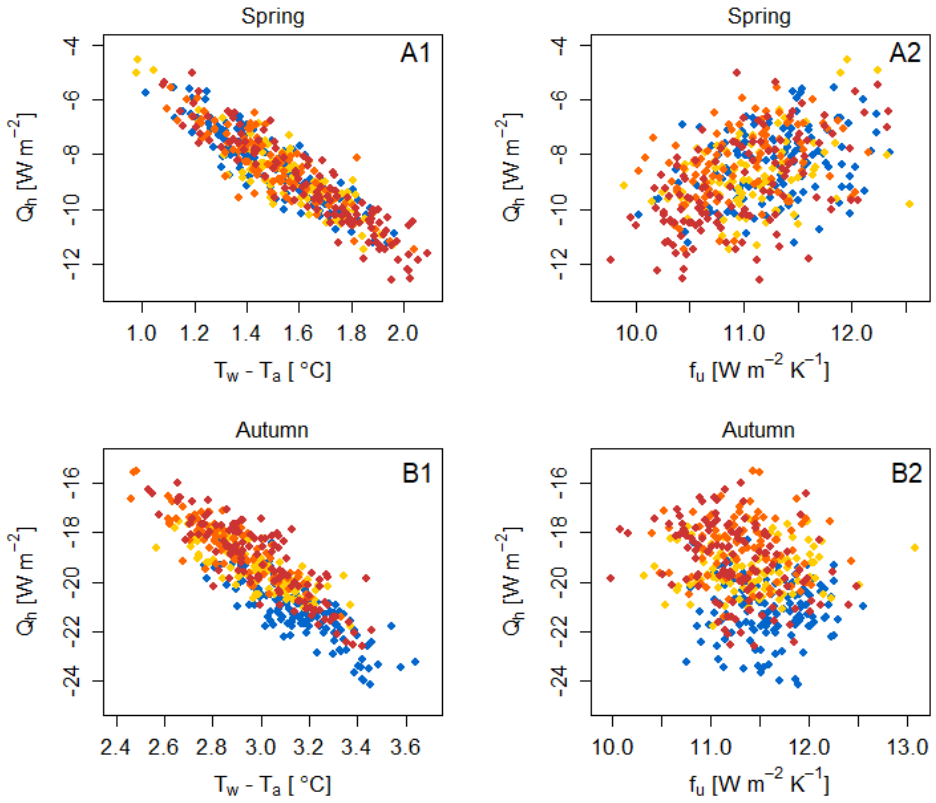

Figure S5.2. 1 Relationship between annual average water-air temperature difference, T_{water}-T_{atm}, and annual average of sensible heat flux, Q_h, in **A** spring and **B** autumn. **2** Relationship between annual average of transfer function, f_u, and annual average of sensible heat flux, Q_h, in **A** spring and **B** autumn. From 1976 to 2099 for PiControl (blue), RCP 2.6 (yellow), RCP 6.0 (orange) and RCP 8.5 (red).

Table S5.2. Summary output from multiple linear regression model used to describe the influence of T_w-T_a and f_u on Q_h in spring. Standardized slope coefficients were calculated to compare the strength of the effect of T_w-T_a and f_u on Q_h. The standardized slope coefficient is measured in units of standard deviation. For example, a β value of 0.6 indicates that a change of 1 standard deviation in the independent variable results in 0.6 standard deviations increase in the dependent variable.

PiControl - Spring					
$Q_h \sim T_w$-T_a					
	unstandardized coefficients		standardized coefficients	t	p-value
	B	std error	β		
(constant)	0.4973	0.42		1.19	>0.05
T_w-T_a	-5.9484	0.28		-21.38	<0.001
R^2 = 0.7893			R_{adj}^2 = 0.7875		
p-value<0.001					
$Q_h \sim (T_w$-$T_a) + f_u$					
	unstandardized coefficients		standardized coefficients	t	p-value
	B	std error	β		

(constant)	4.6010	1.68		2.74	<0.01
T_w-T_a	-6.2914	0.30	-0.9396	-20.66	<0.001
f_u	-0.3181	0.13	-0.1146	-2.52	<0.05
R^2 = 0.7998			R_{adj}^2 = 0.7964		
p-value<0.001					
RCP 2.6 - Spring					
Q_h ~ T_w-T_a					
	unstandardized coefficients		standardized coefficients	t	p-value
	B	std error	β		
(constant)	0.7650	0.42		1.82	>0.05
T_w-T_a	-6.0994	0.28		-22.14	<0.001
R^2 = 0.8007			R_{adj}^2 = 0.7991		
p-value<0.001					
Q_h ~ (T_w-T_a) + f_u					
	unstandardized coefficients		standardized coefficients	t	p-value
	B	std error	β		
(constant)	2.5030	1.78		1.40	>0.05
T_w-T_a	-62782	0.33	-0.9210	-19.14	<0.001
f_u	-0.1317	0.13	-0.0483	-1.00	>0.05
R^2 = 0.8023			R_{adj}^2 = 0.7991		
p-value<0.001					
RCP 6.0 - Spring					
Q_h ~ T_w-T_a					
	unstandardized coefficients		standardized coefficients	t	p-value
	B	std error	β		
(constant)	0.2661	0.43		0.62	>0.05
T_w-T_a	-5.7573	0.29		-19.70	<0.001
R^2 = 0.7608			R_{adj}^2 = 0.7589		
p-value<0.001					
Q_h ~ (T_w-T_a) + f_u					
	unstandardized coefficients		standardized coefficients	t	p-value
	B	std error	β		
(constant)	1.5716	1.84		0.85	>0.05
T_w-T_a	-5.8972	0.35	-0.8934	-16.83	<0.001
f_u	-0.0994	0.14	-0.0386	-0.73	>0.05
R^2 = 0.7619			R_{adj}^2 = 0.7579		
p-value<0.001					
RCP 8.5 - Spring					
Q_h ~ T_w-T_a					
	unstandardized coefficients		standardized coefficients	t	p-value
	B	std error	β		
(constant)	1.2538	0.36		3.47	<0.001

T_w-T_a	-6.3625	0.22		-29.20	<0.001
R^2 = 0.8748			R_{adj}^2 = 0.8738		
p-value<0.001					
$Q_h \sim (T_w$-$T_a) + f_u$					
	unstandardized coefficients		standardized coefficients	t	p-value
	B	std error	β		
(constant)	3.9270	1.67		2.35	<0.05
T_w-T_a	-6.6413	0.28	-0.9763	-24.12	<0.001
f_u	-0.2023	0.12	-0.0663	-1.64	>0.05
R^2 = 0.8775			R_{adj}^2 = 0.8755		
p-value<0.001					

Table S5.3. Summary output from multiple linear regression model used to describe the influence of T_w-T_a and f_u on Q_h in autumn. Standardized slope coefficients were calculated to compare the strength of the effect of T_w-T_a and f_u on Q_h. The standardized slope coefficient is measured in units of standard deviation. For example, a β value of 0.6 indicates that a change of 1 standard deviation in the independent variable results in 0.6 standard deviations increase in the dependent variable.

PiControl - Autumn					
$Q_h \sim T_w$-T_a					
	unstandardized coefficients		standardized coefficients	t	p-value
	B	std error	β		
(constant)	-3.7992	1.12		-3.38	<0.001
T_w-T_a	-5.5165	0.36		-15.53	<0.001
R^2 = 0.664			R_{adj}^2 = 0.6612		
p-value<0.001					
$Q_h \sim (T_w$-$T_a) + f_u$					
	unstandardized coefficients		standardized coefficients	t	p-value
	B	std error	β		
(constant)	16.9486	2.12		7.99	<0.001
T_w-T_a	-6.8972	0.29	-1.0188	-23.93	<0.001
f_u	-1.4134	0.13	-0.4508	-10.59	<0.001
R^2 = 0.8256			R_{adj}^2 = 0.8227		
p-value<0.001					
RCP 2.6 - Autumn					
$Q_h \sim T_w$-T_a					
	unstandardized coefficients		standardized coefficients	t	p-value
	B	std error	β		
(constant)	-5.1669	0.87		-5.83	<0.001
T_w-T_a	-4.8128	0.29		-16.46	<0.001
R^2 = 0.6896			R_{adj}^2 = 0.6870		
p-value<0.001					
$Q_h \sim (T_w$-$T_a) + f_u$					

	unstandardized coefficients		standardized coefficients	t	p-value
	B	std error	β		
(constant)	14.3796	1.29		11.11	<0.001
T_w-T_a	-6.4960	0.19	-1.1208	-33.58	<0.001
f_u	-1.2648	0.08	-0.5460	-16.36	<0.001
R^2 = 0.9033			R_{adj}^2 = 0.9017		
p-value<0.001					

RCP 6.0 - Autumn

$Q_h \sim T_w$-T_a

	unstandardized coefficients		standardized coefficients	t	p-value
	B	std error	β		
(constant)	-0.5160	0.74		-0.70	>0.05
T_w-T_a	-6.2902	0.25		-25.01	<0.001
R^2 = 0.8368			R_{adj}^2 = 0.8354		
p-value<0.001					

$Q_h \sim (T_w$-$T_a) + f_u$

	unstandardized coefficients		standardized coefficients	t	p-value
	B	std error	β		
(constant)	15.5201	1.12		13.86	<0.001
T_w-T_a	-6.8875	0.15	-1.0016	-45.60	<0.001
f_u	-1.2566	0.08	-0.3409	-15.52	<0.001
R^2 = 0.9454			R_{adj}^2 = 0.9445		
p-value<0.001					

RCP 8.5 - Autumn

$Q_h \sim T_w$-T_a

	unstandardized coefficients		standardized coefficients	t	p-value
	B	std error	β		
(constant)	0.0207	1.07		0.02	>0.05
T_w-T_a	-6.3870	0.36		-17.97	<0.001
R^2 = 0.7257			R_{adj}^2 = 0.7234		
p-value<0.001					

$Q_h \sim (T_w$-$T_a) + f_u$

	unstandardized coefficients		standardized coefficients	t	p-value
	B	std error	β		
(constant)	18.58	1.19		15.63	<0.001
T_w-T_a	-6.83	0.19	-0.9113	-36.02	<0.001
f_u	-1.53	0.09	-0.4492	-17.76	<0.001
R^2 = 0.9239			R_{adj}^2 = 0.9227		
p-value<0.001					

Text S5.1. Seasonal relationship between sensible heat flux, Q_h, and water-air temperature difference, T_w-T_a, and transfer function, f_u.

In spring T_w-T_a alone explained between 76-87% of the variation in Q_h whereas the addition of f_u to T_w-T_a explained between 76-95%. The standardized slope coefficients for T_w-T_a [-0.98, -0.89] and f_u [-0.11, -0.04] showed that T_w-T_a had a strong effect on Q_h and f_u has a weak effect on Q_h, and f_u is a non-significant predictor of Q_h. However, in autumn T_w-T_a alone explained between 66-84% of the variation in Q_h whereas the addition of f_u to T_w-T_a explained between 83-94%. The standardized slope coefficients for T_w-T_a [-1.12, -0.91] and f_u [-0.55, -0.34] showed that T_w-T_a has a strong effect on Q_h and f_u had a moderate effect on Q_h and f_u is a significant predictor of Q_h.

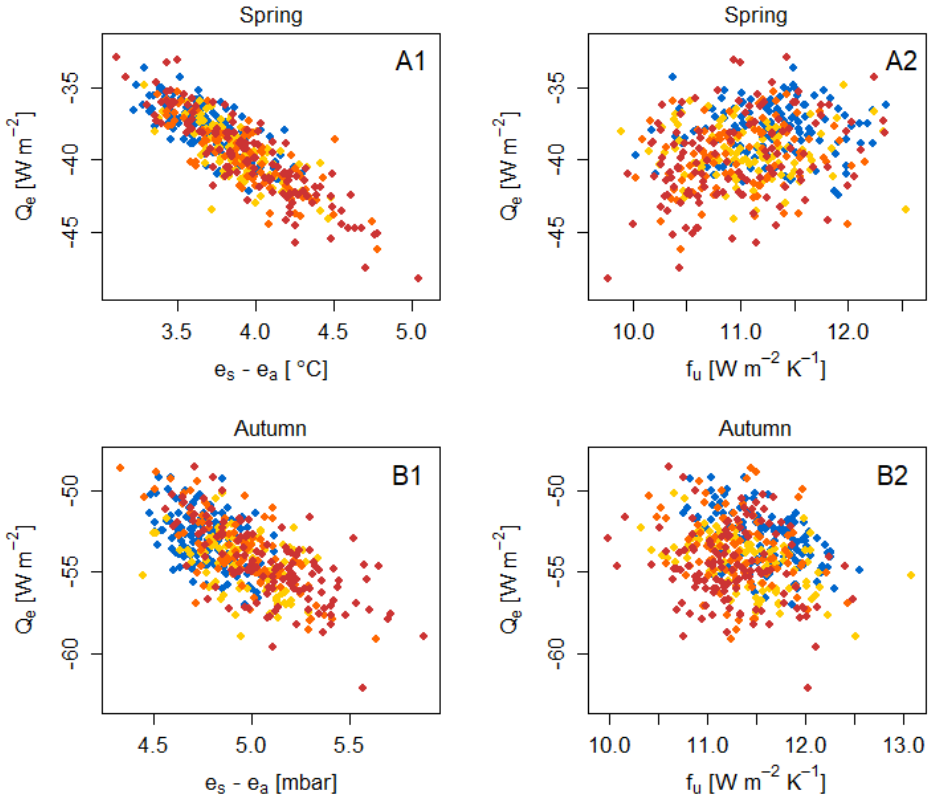

Figure S5.3. 1 Relationship between annual average of vapor pressure deficit, e_s-e_a, and annual average of latent heat flux, Q_e, in **A** spring and **B** autumn. **2** Relationship between annual average of transfer function, f_u, and annual average of latent heat flux, Q_e, in **A** spring and **B** autumn. From 1976 to 2099 for PiControl (blue), RCP 2.6 (yellow), RCP 6.0 (orange) and RCP 8.5 (red).

Table S5.4. Summary output from multiple linear regression model used to describe the influence of e_s-e_a and f_u on Q_e in spring. Standardized slope coefficients were calculated to compare the strength of the effect of e_s-e_a and f_u on Q_e. The standardized slope coefficient is measured in units of standard deviation. For example, a β value of 0.6 indicates that a change of 1 standard deviation in the independent variable results in 0.6 standard deviations increase in the dependent variable.

PiControl - Spring
$Q_e \sim e_s$-e_a

	unstandardized coefficients		standardized coefficients	t	p-value
	B	std error	β		
(constant)	-16.7128	1.66		-10.06	<0.001
e_s-e_a	-5.7238	0.45		-12.81	<0.001
R^2 = 0.5738			R_{adj}^2 = 0.5703		
p-value<0.001					
$Q_e \sim (e_s\text{-}e_a) + f_u$					
	unstandardized coefficients		standardized coefficients	t	p-value
	B	std error	β		
(constant)	15.5308	3.27		4.75	<0.001
e_s-e_a	-8.0032	0.39	-0.9216	-20.62	<0.001
f_u	-2.1071	0.20	-0.4304	-10.59	<0.001
R^2 = 0.7789			R_{adj}^2 = 0.7752		
p-value<0.001					
RCP 2.6 - Spring					
$Q_e \sim e_s\text{-}e_a$					
	unstandardized coefficients		standardized coefficients	t	p-value
	B	std error	β		
(constant)	-13.6028	1.72		-7.90	<0.001
e_s-e_a	-6.6440	0.45		-14.71	<0.001
R^2 = 0.6393			R_{adj}^2 = 0.6364		
p-value<0.001					
$Q_e \sim (e_s\text{-}e_a) + f_u$					
	unstandardized coefficients		standardized coefficients	t	p-value
	B	std error	β		
(constant)	18.0046	3.38		5.33	<0.001
e_s-e_a	-8.7522	0.39	-1.1115	-22.22	<0.001
f_u	-2.1177	0.21	-0.4031	-10.11	<0.001
R^2 = 0.8044			R_{adj}^2 = 0.8012		
p-value<0.001					
RCP 6.0 - Spring					
$Q_e \sim e_s\text{-}e_a$					
	unstandardized coefficients		standardized coefficients	t	p-value
	B	std error	β		
(constant)	-13.6040	1.39		-9.76	<0.001
e_s-e_a	-6.6440	0.36		-18.35	<0.001
R^2 = 0.7341			R_{adj}^2 = 0.7319		
p-value<0.001					
$Q_e \sim (e_s\text{-}e_a) + f_u$					
	unstandardized coefficients		standardized coefficients	t	p-value
	B	std error	β		

(constant)	14.6792	3.61		4.07	<0.001
e_s-e_a	-8.4125	0.36	-1.0848	-23.27	<0.001
f_u	-1.9383	0.24	-0.3842	-8.24	<0.001
R^2 = 0.8297			R_{adj}^2 = 0.8268		
p-value<0.001					
RCP 8.5 - Spring					
Q_e ~ e_s-e_a					
	unstandardized coefficients		standardized coefficients	t	p-value
	B	std error	β		
(constant)	-11.3709	1.31		-8.68	<0.001
e_s-e_a	-7.1964	0.32		-21.93	<0.001
R^2 = 0.7977			R_{adj}^2 = 0.7960		
p-value<0.001					
Q_e ~ (e_s-e_a) + f_u					
	unstandardized coefficients		standardized coefficients	t	p-value
	B	std error	β		
(constant)	19.5691	3.21		6.10	<0.001
e_s-e_a	-9.1588	0.31	-1.1367	-29.49	<0.001
f_u	-2.1123	0.21	-0.3899	-10.12	<0.001
R^2 = 0.8904			R_{adj}^2 = 0.8886		
p-value<0.001					

Table S5.5. Summary output from multiple linear regression model used to describe the influence of e_s-e_a and f_u on Q_e in autumn. Standardized slope coefficients were calculated to compare the strength of the effect of e_s-e_a and f_u on Q_e. The standardized slope coefficient is measured in units of standard deviation. For example, a β value of 0.6 indicates that a change of 1 standard deviation in the independent variable results in 0.6 standard deviations increase in the dependent variable.

PiControl - Autumn					
Q_e ~ e_s-e_a					
	unstandardized coefficients		standardized coefficients	t	p-value
	B	std error	β		
(constant)	-30.4175	4.22		-7.21	<0.001
e_s-e_a	-4.7449	0.88		-5.36	<0.001
R^2 = 0.1908			R_{adj}^2 = 0.1841		
p-value<0.001					
Q_e ~ (e_s-e_a) + f_u					
	unstandardized coefficients		standardized coefficients	t	p-value
	B	std error	β		
(constant)	32.6393	4.03		8.11	<0.001
e_s-e_a	-8.9437	0.51	-0.8233	-17.66	<0.001
f_u	-3.7107	0.20	-0.8650	-18.56	<0.001
R^2 = 0.7896			R_{adj}^2 = 0.7862		

p-value<0.001					
RCP 2.6 - Autumn					
$Q_e \sim e_s\text{-}e_a$					
	unstandardized coefficients		standardized coefficients	t	p-value
	B	std error	β		
(constant)	-28.6578	3.76		-7.62	<0.001
$e_s\text{-}e_a$	-5.1309	0.74		-6.72	<0.001
$R^2 = 0.2704$			$R_{adj}^2 = 0.2644$		
p-value<0.001					
$Q_e \sim (e_s\text{-}e_a) + f_u$					
	unstandardized coefficients		standardized coefficients	t	p-value
	B	std error	β		
(constant)	38.8668	3.13		12.40	<0.001
$e_s\text{-}e_a$	-9.8106	0.36	-0.9942	-26.91	<0.001
f_u	-3.8917	0.16	-0.9132	-24.71	<0.001
$R^2 = 0.8793$			$R_{adj}^2 = 0.8774$		
p-value<0.001					
RCP 6.0 - Autumn					
$Q_e \sim e_s\text{-}e_a$					
	unstandardized coefficients		standardized coefficients	t	p-value
	B	std error	β		
(constant)	-17.2891	2.93		-5.89	<0.001
$e_s\text{-}e_a$	-7.3545	0.60		-12.35	<0.001
$R^2 = 0.5554$			$R_{adj}^2 = 0.5518$		
p-value<0.001					
$Q_e \sim (e_s\text{-}e_a) + f_u$					
	unstandardized coefficients		standardized coefficients	t	p-value
	B	std error	β		
(constant)	39.3458	3.00		13.10	<0.001
$e_s\text{-}e_a$	-10.0950	0.31	-1.0230	-33.09	<0.001
f_u	-3.7976	0.18	-0.6534	-21.14	<0.001
$R^2 = 0.9053$			$R_{adj}^2 = 0.9037$		
p-value<0.001					
RCP 8.5 - Autumn					
$Q_e \sim e_s\text{-}e_a$					
	unstandardized coefficients		standardized coefficients	t	p-value
	B	std error	β		
(constant)	-25.8524	2.91		-8.87	<0.001
$e_s\text{-}e_a$	-5.6439	0.57		-9.88	<0.001
$R^2 = 0.4447$			$R_{adj}^2 = 0.4401$		
p-value<0.001					
$Q_e \sim (e_s\text{-}e_a) + f_u$					

	unstandardized coefficients		standardized coefficients	t	p-value
	B	std error	β		
(constant)	37.9946	3.39		11.20	<0.001
e_s-e_a	-9.2203	0.32	-1.0894	-28.70	<0.001
f_u	-4.0545	0.20	-0.7814	-20.59	<0.001
R^2 = 0.8767			R_{adj}^2 = 0.8746		
p-value<0.001					

Text S5.2. Seasonal relationship between latent heat flux Q_e and vapor pressure deficit e_s-e_a and transfer function f_u.

In spring e_s-e_a alone explained between 66-84% of the variation in Q_e whereas the addition of f_u to e_s-e_a explained between 83-94%. The standardized slope coefficients for e_s-e_a [-1.12, -0.91] and f_u [-0.55, -0.33] showed that e_s-e_a had a strong effect on Q_e and f_u has a moderate effect on Q_e. However, in autumn e_s-e_a alone explained between 19-56% of the variation in Q_e whereas the addition of f_u to e_s-e_a explained between 79-91%. The standardized slope coefficients for e_s-e_a [-1.09, -0.82] and f_u [-0.91, -0.65] showed that e_s-e_a and f_u had a strong effect on Q_e.